



On Whistler Mode Wave Relation to Electron Field-Aligned Plateau Populations

A. V. Artemyev¹  and D. Mourenas²¹Institute of Geophysics and Planetary Physics, University of California, Los Angeles, Los Angeles, CA, USA, ²CEA, DAM, DIF, Arpajon, France**Key Points:**

- Plateau electron populations are often unlikely to be formed by acceleration through Landau resonance with whistler mode waves alone
- Field-aligned electric fields carried by kinetic Alfvén waves and electrostatic noise are good candidates for electron plateau formation
- A weak damping of whistlers in Landau resonance with preexisting electron plateau populations likely determines their predominant observations

Correspondence to:A. V. Artemyev,
aartemyev@ucla.igpp.edu**Citation:**Artemyev, A. V., & Mourenas, D. (2020). On whistler mode wave relation to electron field-aligned plateau populations. *Journal of Geophysical Research: Space Physics*, 125, e2019JA027735. <https://doi.org/10.1029/2019JA027735>

Received 15 DEC 2019

Accepted 24 FEB 2020

Accepted article online 28 FEB 2020

Abstract Whistler mode waves are among the most intense electromagnetic emissions and play an important role in the energy redistribution between electron populations in the Earth inner magnetosphere through wave-particle resonant interactions. Usually generated by transversely anisotropic plasma sheet electron populations ($\sim 10\text{--}30$ keV) through cyclotron resonance, whistler mode waves can effectively accelerate a small fraction of the seed population of energetic electrons (~ 100 keV) up to relativistic energies. However, these waves can be efficiently damped through simultaneous interactions with much more numerous suprathermal electrons ($\sim 0.1\text{--}1$ keV) via Landau resonance. Recent observations indeed show that electron distributions accompanied by intense whistler mode emissions often contain a plateau-like electron population at energies close to the energy of Landau resonance with the waves. However, simultaneous observations of these waves and of the related plateau population does not prove a causal relationship. Here, we test the hypothesis that such a plateau population may have been formed by whistler mode waves generated earlier, or by other types of waves. Combining analytical estimates and spacecraft observations, we show that this plateau population is often unlikely to be formed by whistler mode waves alone. We suggest three alternative scenarios that can lead to the formation of plateau populations and test these scenarios based on spacecraft observations. We show that a plateau population can be formed by ultralow frequency electric fields (carried by kinetic Alfvén waves or time domain structures) often accompanying injections of plasma sheet electrons—the energy source for whistler mode waves. We also discuss the possible role of ionospheric secondary electrons.

1. Introduction

Whistler mode waves are intense electromagnetic waves observed in the inner magnetosphere (Agapitov et al., 2013; Li et al., 2011; Meredith et al., 2012; Tsurutani & Smith, 1979), in the near-Earth plasma sheet (Khotyaintsev et al., 2011; Zhang et al., 2018), at the Earth's magnetopause (Le Contel et al., 2016; Wilder et al., 2016), bow shock (Wilson et al., 2014), and in the solar wind (Tong et al., 2019). With frequencies below (but comparable with) electron cyclotron frequency, these waves are excited by electron thermal anisotropy (Sagdeev & Shafranov, 1961) or electron flow anisotropy (Gary & Feldman, 1977; Gary & Li, 2000; Vasko et al., 2019). Their generation and resonant interaction with electron result in a relaxation of the initially anisotropic electron distribution (Galeev & Sagdeev, 1979; Gary & Wang, 1996; Kuzichev et al., 2019; Tao et al., 2017) and in a significant electron acceleration (e.g., Thorne et al., 2013, and references therein). The importance of whistler mode waves for the description of electron dynamics has sparked a lot of very detailed experimental and theoretical investigations (see, e.g., recent reviews by Albert et al., 2013; Artemyev et al., 2016; Millan & Thorne, 2007; Ni et al., 2016; Omura et al., 2013; Shklyar & Matsumoto, 2009; Thorne, 2010).

The transversely anisotropic electron distributions naturally produced in the inner magnetosphere and plasma sheet (An et al., 2017; Yue et al., 2016; Zhang et al., 2018) tend to generate whistler mode waves with field-aligned wave number—for which the wave growth rate is the largest (Fu et al., 2014; Kennel et al., 1970; Summers et al., 2013). However, wave propagation in an inhomogeneous geomagnetic field results in wave vector divergence (Bortnik et al., 2006; Katoh, 2014; Kimura, 1966; Lundin & Krafft, 2001; Shklyar et al., 2004), and oblique whistler mode waves are often observed in the inner magnetosphere (Agapitov et al., 2013, 2018; Li, Santolik, et al., 2016; Santolik et al., 2009; Zhou et al., 2019). The main difference between field-aligned and oblique waves of fixed frequency is the energy range of resonant electrons: field-aligned lower-band chorus waves below half the electron gyrofrequency resonate with >10 keV electrons through

cyclotron resonance, whereas oblique lower-band chorus waves can resonate with much colder electrons through the Landau resonance (e.g., Shklyar & Matsumoto, 2009, and references therein). Waves generated by cyclotron resonance with transversely anisotropic electrons can principally be damped through Landau resonance with lower-energy electrons (Shklyar, 2011b, 2017), providing an energy transfer from hot to cold particles. Such a process may modify the shape of the electron distribution and, thus, can change the properties of the generated waves (as suggested by Li et al., 2019; Ratcliffe & Watt, 2017). Indeed, a series of observations report the formation of electron plateau populations (i.e., with a very weak local gradient of their field-aligned velocity distribution) around energies of Landau resonance with whistler mode waves (Agapitov et al., 2016; Chen et al., 2019; Li, Mourenas, et al., 2016; Min et al., 2014). Therefore, there is an open question: Can whistler mode waves form this plateau electron population themselves?

Formally speaking, this question can be addressed by numerical simulations of whistler mode wave generation and resonant interaction with electrons. However, the overwhelming majority of such simulations consider whistler mode waves that cannot deviate from the field-aligned propagation (e.g., Fu et al., 2014; Katoh & Omura, 2007, 2013; Lu et al., 2010; Tao, 2014). At the present time, only a limited number of 2-D simulations have been performed in an inhomogeneous magnetic field (required to consider realistic oblique waves) and the question of plateau formation was generally not considered in these simulations (Agapitov et al., 2018; Drake et al., 2015; Katoh & Omura, 2016; Ke et al., 2017; Kuzichev et al., 2019). Only two simulations have yet described a plateau formation. A 2-D simulation in a homogeneous magnetic field from Ratcliffe and Watt (2017) indicated the formation of a plateau following the linear growth of oblique waves at half the cyclotron frequency (where waves can reach both cyclotron and Landau resonance with electrons), but the initial amplitudes of the waves were already high due to numerical noise. A 1-D simulation in a homogeneous magnetic field (Li et al., 2019) has also shown a self-consistent formation of a plateau via parallel electron acceleration by oblique chorus waves, the corresponding local reduction of temperature anisotropy suppressing wave growth at half the cyclotron frequency and leading to separate lower-band and upper-band chorus waves (a similar mechanism of anisotropy reduction was considered by Agapitov et al. (2016) to explain the usual absence of intense parallel lower-band chorus waves when intense very oblique lower-band waves are present). In the simulation, however, the coordinate system was rotated to generate oblique waves in a 1-D setup, thereby excluding the generation of the most unstable field-aligned waves; moreover, the considered initial temperature anisotropy was much larger than that in observations (Li et al., 2019).

Why is this question of the formation of an electron plateau distribution so important? Whistler mode waves are known to provide an energy cascade from energetic (10 – 100 keV in the inner magnetosphere) anisotropic electron populations (provided by plasma injections Tao et al., 2011; Zhang et al., 2018 or inner magnetosphere compression by the solar wind Li et al., 2015; Yue et al., 2017) to relativistic and ultrarelativistic energies (Horne et al., 2005; Thorne et al., 2013). But if most of the anisotropic electron energy (the free energy for wave generation) is expended for plateau formation (i.e., transferred to cold electrons), then the efficiency of these waves in relativistic electron acceleration could be significantly reduced. The question of plateau formation (or not) by whistler mode waves is part of the bigger question about the actual wave energy budget available for relativistic electron acceleration. Therefore, the formation of electron plateau distributions observed simultaneously with whistler mode waves (Chen et al., 2019; Li, Mourenas, et al., 2016; Min et al., 2014) requires more investigations.

In this paper, we consider this question using energy conservation and entropy growth laws, combined with simultaneous wave and plasma measurements. We check whether the initial, transversely anisotropic electron distribution can be transformed into a distribution including a plateau population in such a way that it results in an increase of total entropy of the system and a conservation of total energy. We provide several analytical estimates and consider electron distributions recorded within short time intervals of intense whistler mode wave observations. The main conclusion of our analysis is that the plateau population is often unlikely to be formed by whistler mode waves generated earlier and that, on the contrary, a preexisting plateau population can significantly reduce wave damping and, therefore, determine the characteristics of the fastest-growing whistler mode waves. We also examine several alternative mechanisms that could explain the formation of the plateau electron populations observed during the same time intervals as whistler mode emissions.

2. Theoretical Estimates

To simplify estimates, we consider the transformation of a single anisotropic Maxwellian distribution $f_{\text{init}} = C_0 \exp(-mv_{\parallel}^2/2T_{0\parallel} - mv_{\perp}^2/2T_{0\perp})$ into a combination of an anisotropic Maxwellian distribution and a beam distribution $f_{\text{final}} = \delta C_1 \exp(-mv_{\parallel}^2/2T_{1\parallel} - mv_{\perp}^2/2T_{1\perp}) + (1 - \delta)C_2 \exp(-mv_{\perp}^2/2T_2) \cdot \sum_{\pm} \exp(-m(v_{\parallel} \pm v_D)^2/2T_2)/2$ where $C_i = n(2\pi T_{i\parallel}/m)^{-3/2}(T_{i\perp}/T_{i\parallel})^{-1}$, and n is the initial density of hot particles (that is much smaller than the total density n_0 including the cold particle population). This transformation assumes that (1) f_{init} is unstable to whistler mode wave generation through cyclotron resonance (Sagdeev & Shafranov, 1961); (2) whistler mode waves, being generated around the equatorial plane, propagate along curved magnetic field lines with an increase of their wave normal angle along propagation (Shklyar et al., 2004); (3) oblique whistler mode waves interact with electrons through Landau resonance and get damped at high latitudes (Bortnik et al., 2006; Chen et al., 2013); (4) this Landau resonant interaction results in a generation of electron beams with $v_D \simeq v_{\text{Landau}} = \omega/k_{\parallel}$; (5) the scattering of cyclotron resonant electrons (with parallel velocity $v_{\text{Cyclotron}} = (\omega - \Omega_{\text{ce}})/k_{\parallel}$) by the generated wave results in an isotropization of the electron distribution (Gary, 2005). Therefore, there are three input parameters of the system, $(T_{0\parallel}, A_0 = T_{0\perp}/T_{0\parallel}, \beta_{\text{init}\parallel} = 8\pi n T_{0\parallel}/B_{\text{bg}}^2)$, and five output parameters: $T_{1\parallel}, A_1 = T_{1\perp}/T_{1\parallel}, T_2, v_D$, and δ (note that $\beta_{\text{final}\parallel} = \beta_{\text{init}\parallel} T_{\text{final}\parallel}/T_{0\parallel}$, where $T_{\text{final}\parallel} = \delta T_{1\parallel} + (1 - \delta)(T_2 + mv_D^2)$ is the parallel temperature of the final distribution). At first sight, such a large number of free parameters (three inputs and five outputs) seems to prevent us from checking whether this transformation is possible. However, there are actually five constraints that allow to exclude all the final parameters. Let us consider below these five constraints.

In this set of assumptions, the wave damping requires additional clarification. Although the damping rate can be calculated for local plasma parameters, in the radiation belts wave damping is a spatial rather than a temporal effect: waves propagating along magnetic field lines are usually almost fully damped when they reach the lower-hybrid resonance at magnetic latitudes $\sim 30\text{--}40^\circ$, and the intensity of reflected waves (propagating from high latitudes toward the equator) is quite small (e.g., Agapitov et al., 2013). High-latitude observations suggest that wave damping is also associated with the loss of wave coherence (Tsurutani et al., 2013). These two effects result in a decrease of the efficiency of wave-particle interaction with waves at high latitudes (as well as with reflected waves) and, thus, such waves could not contribute significantly to the isotropization of the electron distributions. In other words, we can assume that there is no electron scattering by reflected waves and that the typical lifetime of wave packets is less than a quarter of the wave bounce period along field lines. In the future, full numerical simulations (including ray tracing with hot plasma effects, see Breuillard et al., 2013; Chen et al., 2013; Maxworth & Golkowski, 2017, and Watt et al., 2013) will be needed to take into account, in more detail, the latitudinal and azimuthal distributions of wave damping.

2.1. Maximum Growth Rate of Whistler Mode Wave Generation

In the approximation of the cold plasma with a small population of resonant particles (i.e., when n is much smaller than the cold plasma density), the whistler mode wave growth rate is given by this equation (Kennel et al., 1970):

$$\gamma = \pi^2 \frac{(\Omega_{\text{ce}} - \omega)^3}{k\Omega_{\text{ce}}n_0} \left(\int_0^\infty v_{\perp}^2 \left(\frac{\partial f}{\partial v_{\perp}} - \frac{v_{\perp}}{v_{\parallel}} \frac{\partial f}{\partial v_{\parallel}} \right) dv_{\perp} - \frac{\omega}{\Omega_{\text{ce}} - \omega} \int_0^\infty v_{\perp} f dv_{\perp} \right)_{v_{\parallel}} = v_{\text{Cyclotron}} \quad (1)$$

where n_0 is the total plasma density (generally larger than hot electron density n). For a sufficiently dense plasma with $\omega_{\text{pe}}^2 \gg \Omega_{\text{ce}}^2$ (with ω_{pe} and Ω_{ce} the electron plasma frequency and gyrofrequency) and parallel wave propagation, the cold plasma dispersion can be simplified to $\omega = \Omega_{\text{ce}}(1 + (\omega_{\text{pe}}/kc)^2)^{-1}$ (e.g., Shklyar et al., 2004). Substituting f_{init} into equation (1), we obtain the wave growth rate

$$\gamma = \frac{\sqrt{\pi}}{2} \frac{(\Omega_{\text{ce}} - \omega)^3 n}{k\sqrt{2T_{0\parallel}}/m\Omega_{\text{ce}}n_0} \left(\left(\frac{T_{0\perp}}{T_{0\parallel}} - 1 \right) - \frac{\omega}{\Omega_{\text{ce}} - \omega} \right) \exp\left(-\frac{mv_{\text{Cyclotron}}^2}{2T_{0\parallel}}\right) \quad (2)$$

shown in Figure 1b. For given input parameters $(T_{0\parallel}, A_0 = T_{0\perp}/T_{0\parallel}, \beta_{\text{init}\parallel})$, the condition that the waves are generated with the maximum growth rate can be written as $\omega = \omega^*(T_{0\parallel}, A_0, \beta_{\text{init}\parallel})$ and, thus, the Landau resonant velocity is $v_{\text{Landau}} = \omega^*/k_{\parallel} = v_{\text{Landau}}(T_{0\parallel}, A_0, \beta_{\text{init}\parallel})$. Therefore, the beam velocity $v_D \approx v_{\text{Landau}}$ in f_{final} is a function of the system input parameters (see Figure 1c). Note that this approximation holds only for low to moderate wave amplitudes, whereas for intense waves (e.g., high-amplitude chorus) a more

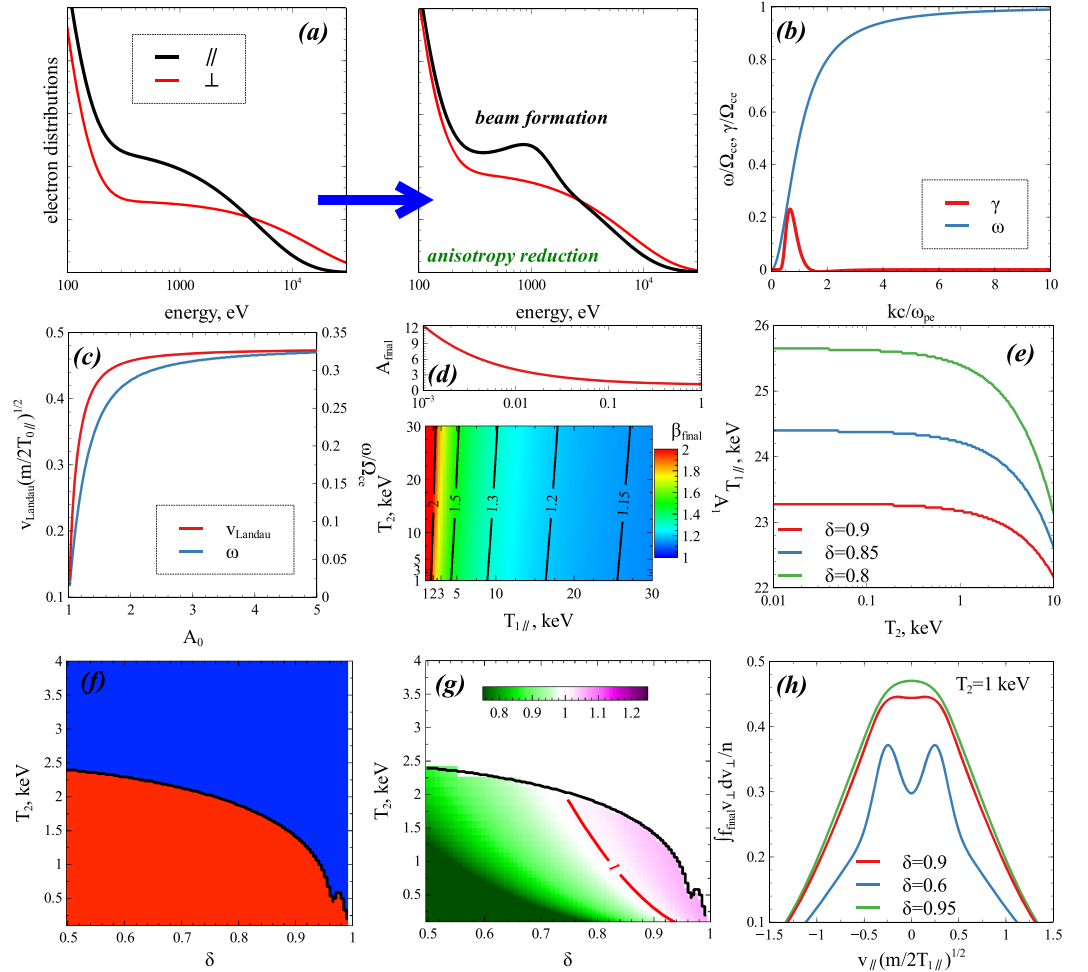


Figure 1. (a) Scheme of evolution of particle distribution function: from transversely anisotropic electrons to beam formation and anisotropy reduction. (b) Whistler mode wave growth rate and dispersion relation (note that the growth rate is normalized to the ratio n/n_0 of hot electron density to total plasma density). (c) Landau velocity of the fastest growing waves as a function of A_0 for $T_{0\parallel} = 10$ keV and three values of $\beta_{\text{init}\parallel}$. (d) Condition of the whistler mode wave marginal stability $A_{\text{final}} = 1 + a\beta_{\text{final}\parallel}^b$ (top) and $A_1 = A_1(T_{1\parallel}, T_2)$ for $\beta_{\text{init}\parallel} = 1$ and $\delta = 0.9$; (e) $T_{1\parallel}$ as a function of T_2 for different δ and A_1 given by equation (3), $v_D = v_{\text{Landau}}$. (f) Parametric regions (in (δ, T_2) space) with f_{final} having plateau (red) and without plateau (blue); A_1 given by equation (3), $v_D = v_{\text{Landau}}$, $T_{1\parallel}$ given by energy conservation. (g) Ratio of entropies of the final and initial electron distributions in (δ, T_2) space. The black curve shows the parametric boundary from panel (f). (h) Three distribution functions f_{final} for $T_2 = 1$ keV: $\delta = 0.9$ corresponds to a distribution with a final entropy larger than the initial entropy and with plateau, $\delta = 0.6$ corresponds to a distribution with final entropy larger than initial entropy and with beams (potential plateau); $\delta = 0.95$ corresponds to a distribution with final entropy smaller than the initial entropy. For all the displayed calculations, we use $A_0 = 3$, $T_{0\parallel} = 10$ keV, $\beta_{\text{init}\parallel} = 1$, if other values are not given inside the figure.

comprehensive analysis of nonlinear wave growth rates would be required (Omura et al., 2008, 2013; Shklyar & Matsumoto, 2009)

2.2. Marginally Stable Electron Distribution

The final electron distribution f_{final} should be nearly stable to whistler mode wave generation, that is, the relaxation of the initially unstable distribution f_{init} should stop when no waves with significant amplitudes can be generated anymore. The parameters of the marginally stable distribution satisfy the equation $A_{\text{final}} = 1 + a\beta_{\text{final}\parallel}^b$ with A the temperature anisotropy, $a \approx 0.21$, $b \approx 0.58$ (Gary, 2005; Gary & Wang, 1996). The parameter A_{final} is given by the following equation (Figure 1d):

$$A_{\text{final}} = \frac{\delta T_{1\perp} + (1 - \delta) T_2}{\delta T_{1\parallel} + (1 - \delta) (T_2 + mv_D^2)} = \frac{\delta A_1 + (1 - \delta) T_2 / T_{1\parallel}}{\delta + (1 - \delta) (T_2 + mv_D^2) / T_{1\parallel}} \quad (3)$$

Therefore, for given $T_{0\parallel, A_0, \beta_{\text{init}\parallel}}$, we obtain a constraint $A_1 = A_1(T_{1\parallel, T_2, \delta})$, that is, the condition of marginal stability reduces the number of output parameters. Note that the considered threshold for a marginally stable distribution $A_{\text{final}} = 1 + a\beta_{\text{final}\parallel}^{-b}$ has been obtained for broadband low-amplitude waves in a homogeneous magnetic field (Gary & Wang, 1996; Gary, 2005), that is, this equation is not guaranteed to hold for whistler mode waves in the inner magnetosphere. Nevertheless, several observational studies have confirmed that $A_{\text{final}} = 1 + a\beta_{\text{final}\parallel}^{-b}$ is a reasonable approximation in the inner magnetosphere and in plasma injection regions (Yue et al., 2016; Zhang et al., 2018).

2.3. Energy Conservation

Whistler mode wave generation/amplification via cyclotron resonance with hot particles (at $v_{\parallel} \approx v_{\text{Cyclotron}} = (\omega - \Omega_{ce})/k_{\parallel}$) and wave damping by Landau resonance with cold particles (at $v_{\parallel} = v_{\text{Landau}} = \omega/k_{\parallel}$) can be considered as an energy transfer between these two populations (Shklyar, 2011b, 2017), such that the wave energy remains a negligible fraction of the transferred energy (Shklyar, 2011a). This last condition allows us to write the conservation of total energy in the system under the form $nT_{0\parallel}(1 + 2A_0) \approx \delta nT_{1\parallel}(1 + 2A_1) + (1 - \delta)n(3T_2 + mv_D^2)$, where $v_D = v_{\text{Landau}}$ and $A_1 = A_1(T_2, T_{1\parallel}, \delta)$. Therefore, energy conservation determines $T_{1\parallel}$ as a function of the input parameters ($T_{0\parallel}, A_0$) and output parameters T_2, δ (see Figure 1e).

2.4. Plateau Formation

The final distribution f_{final} considered here should contain a plateau in the parallel velocity space. We slightly relax this criterion and consider an f_{final} comprising not necessarily a plateau but at least electron beams, because such beams should quickly (on plasma time scales) relax to plateaus through the excitation of electrostatic waves (Vedenov, 1967). Full numerical simulations have indeed demonstrated the relaxation of electron beams over typical time scales of tens of inverse plasma frequencies (see, e.g., Fu et al., 2014; Gary et al., 2000, and reference therein). Moreover, electrons scattering by whistler mode waves may also contribute to beam relaxation and plateau formation (e.g., An et al., 2017; Zhang et al., 1993, and references therein). Accordingly, we require that the equation $\partial \int f_{\text{final}} v_{\perp} dv_{\perp} / \partial v_{\parallel} = 0$ should have three roots: one root is the peak of the distribution around zero velocities, and the two other roots are for the two symmetrical beams or plateaus. We take into account that A_1, v_D and $T_{1\parallel}$ are determined by the above constraints of marginal stability of the final distribution ($A_1 = A_1(T_2, T_{1\parallel}, \delta)$), maximum growth rate of whistler mode waves ($v_D = v_{\text{Landau}}$), and energy conservation ($T_{1\parallel} = T_{1\parallel}(T_2, \delta)$). As a result, the three roots of equation $\partial \int f_{\text{final}} v_{\perp} dv_{\perp} / \partial v_{\parallel} = 0$ determine a region in 2-D space of (δ, T_2) (see Figure 1f) where plateau and beams can be formed for a wide range of δ and sufficiently small T_2 values.

2.5. Entropy Increase

For given input parameters, the four aforementioned constraints define $v_D, A_1, T_{1\parallel}$ and determine a parametrical region in (δ, T_2) space. To further constrain the range of (δ, T_2) values, we use the concept of entropy increase inside a closed system, this system consisting here of an electron distribution trapped along a curved geomagnetic field line. Assuming a spontaneous evolution of the electron distribution within the considered closed system (without external forces), the entropy of f_{final} should be larger than, or equal to, the entropy of f_{init} :

$$S_{\text{final}} = - \int_{-\infty}^{+\infty} \ln(f_{\text{final}}) f_{\text{final}} dv_{\parallel} \int_0^{\infty} v_{\perp} dv_{\perp} \geq S_{\text{init}} = - \int_{-\infty}^{+\infty} \ln(f_{\text{init}}) f_{\text{init}} dv_{\parallel} \int_0^{\infty} v_{\perp} dv_{\perp} \quad (4)$$

The inequality in equation (4) defines a prohibited range of (δ, T_2) values. Figure 1g show $s = S_{\text{init}}/S_{\text{final}}$ in the (δ, T_2) space. The requirement of an increase of entropy is found to significantly shrink the range of available (δ, T_2) values. Only large δ values remain acceptable, corresponding to small beams.

Note that we assume a closed system, where no new electron injection occurs during the very fast evolution of the initial distribution. We further assume that the initially generated wave creates the beam via Landau damping and gets fully damped at high latitude in the final state.

In low-latitude satellite observations, one may rather observe the *nearly* final electron distribution of entropy, $S_{\text{el,obs}}^{\text{final}}$, together with a not yet fully damped wave of entropy, $S_{\text{wave}}^{\text{final}}$. In this case, the entropy change is not exactly $\Delta S = S_{\text{el,obs}}^{\text{final}} - S_{\text{el}}^{\text{init}}$, but rather $\Delta S = (S_{\text{el,obs}}^{\text{final}} - S_{\text{el}}^{\text{init}}) + (S_{\text{wave}}^{\text{final}} - S_{\text{el(wave)}}^{\text{init}})$, with $S_{\text{el(wave)}}^{\text{init}}$ the entropy of the small portion of the initial electron distribution that has transferred its energy to the observed wave. But $S_{\text{wave}}^{\text{final}}$ and $S_{\text{el(wave)}}^{\text{init}}$ are the final and initial entropies of the same bunch of energy transferred from particles

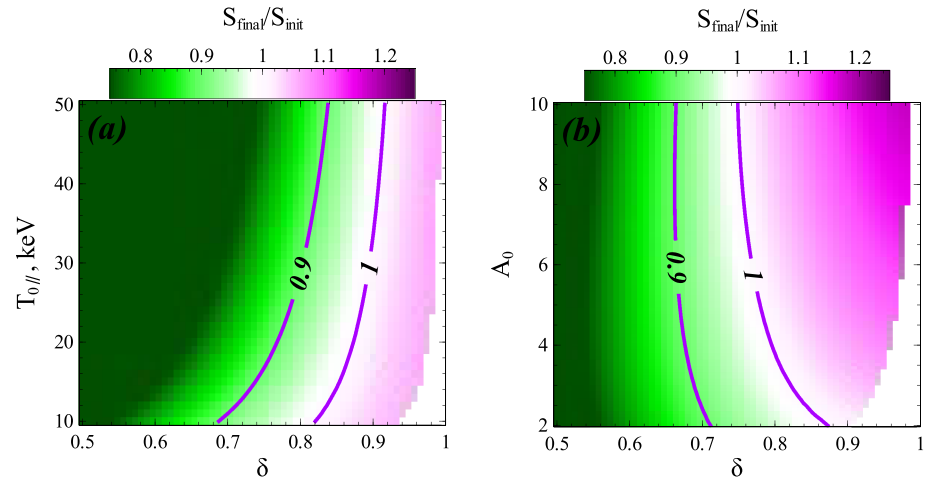


Figure 2. Ratio of final to initial entropy of the electron distribution for the parameters of plateau (or beam) formation: (a) $A_0 = 3$, $\beta_{\text{init}\parallel} = 1$, $T_2 = 1$ keV; (b) $T_{0\parallel} = 10$ keV, $\beta_{\text{init}\parallel} = 1$, $T_2 = 1$ keV. A_1 is given by equation (3), $v_D = v_{\text{Landau}}$, $T_{1\parallel}$ is provided by energy conservation.

to wave, implying $S_{\text{wave}}^{\text{final}} \sim S_{\text{el(wave)}}^{\text{init}}$. Moreover, Shklyar (2011a) has shown that the wave is only a mediator in the energy transfer between initial and final electron populations, wave energy remaining a negligible fraction of the total transferred electron energy. Accordingly, $(S_{\text{wave}}^{\text{final}} - S_{\text{el(wave)}}^{\text{init}})$ can be neglected compared with $(S_{\text{el,obs}}^{\text{final}} - S_{\text{el}}^{\text{init}})$.

2.6. Parametric Investigation

Figure 1h shows three distributions f_{final} obtained for $A_0 = 3$, $T_{0\parallel} = 10$ keV, and $\beta_{\text{init}\parallel} = 1$, A_1 given by equation (3), $v_D = v_{\text{Landau}}$, $T_{1\parallel}$ given by energy conservation. The distribution for $\delta = 0.65$ corresponds to strong beams, and the formation of such beams decreases the system entropy, that is, this distribution cannot be formed spontaneously during a self-consistent evolution. The distribution for $\delta = 0.95$ does not contain any beams or plateau, that is, this distribution is beyond the scope of the parametric region of our interest. The distribution for $\delta = 0.9$ contains weak beams (or plateaus) and the entropy of this distribution is higher than the entropy of the initial distribution, that is, the formation of such a distribution satisfies all our requirements. For any input parameters $(T_{0\parallel}, A_0, \beta_{\text{init}\parallel})$, we can therefore determine the range of (δ, T_2) for which the transformation shown in Figure 1a is physically possible, by using five different constraints that define or limit the values of the output parameters.

Let us explore the ranges of initial parameters for which this transformation is possible. We fix $T_1 = 1$ keV (a typical temperature for observed plateaus/beams, see Li, Mourenas, et al., 2016; Li et al., 2019, Min et al., 2014) and vary the initial $T_{0\parallel} \in [10, 50]$ keV (typical temperature of anisotropic electrons in the injection region, Zhang et al., 2018, and inner magnetosphere, Demekhov et al., 2017; Fu et al., 2014; Li, Mourenas, et al., 2016), A_0 . Figure 2 shows these parametric regions in the $(T_{0\parallel}, \delta)$ and (A_0, δ) spaces. Both $T_{0\parallel}$ and A_0 have a weak influence on the range of δ where entropy grows and plateau/beam can be formed. The range of δ with $S_{\text{final}}/S_{\text{init}} > 1$ is quite narrow and only corresponds to distributions with beam density below 20% of the hot electron density (especially for the realistically moderate anisotropy). Taking into account that many approximations have been made to plot Figure 2, we also show the permitted δ range for the relaxed condition $S_{\text{final}}/S_{\text{init}} > 0.9$, for which the beam density can reach up to 30% of the hot electron density.

For realistic systems, therefore, the main role should be played by the energy conservation equation. Accordingly, we can start from the observed electron distribution with a plateau/beam and assume that it is marginally stable (with A_1 close to the marginal stability threshold), and then transfer the entire plateau/beam energy into the energy of the initial anisotropic distribution: although this inverse transformation can likely be performed with a decrease of entropy, the reconstructed initial distribution may easily turn out to be unrealistically energetic or unstable (e.g., $T_{0\parallel}$ exceeding a reasonable range, or A_0 well exceeding realistic levels). In the next section, we check the parameters of reconstructed initial distributions for several events during which final electron distributions with plateaus have been observed (note that the

evolution of the unstable initial electron distribution is generally sufficiently fast to prevent its observation by satellites; e.g., see Fu et al., 2014).

3. Applications to Observed Electron Distributions

We examine four events of electron plateau observations in the presence of whistler mode chorus waves, to check if these plateaus could have been formed by such whistler mode waves. In each case, we fit both transverse and parallel electron phase space densities (PSD) by combinations of Maxwellian and Kappa distributions, and calculate the drift energy density of the electron beam corresponding to the observed plateau $E_{\text{Drift,beam}} = n_{\text{beam}} m_e v_{D,\text{final}}^2$ (for the two symmetric beams). Next, we transfer this (final) beam drift energy back to the (initial) transverse energy of the anisotropy of the electron population that could potentially generate, via cyclotron resonance, the observed waves in Landau resonance with the beam. Hereafter, Landau resonance and wave growth rate are calculated using the full formulae for oblique whistler mode waves (Artemyev et al., 2016), based on the wave normal angle of the observed chorus wave. To ensure exact conservation of total electron density, we delete in the reconstructed (initial) distribution the final beam, but add an *initial* beam population of the same density (representing electrons that have been accelerated by chorus waves) of similar temperature and initial drift velocity $v_{D,\text{init}} = 0$. Finally, we calculate the difference $S_{\text{final}} - S_{\text{init}}$ between the observed (final) and estimated (initial) entropies of the electron distribution, normalized to the entropy S_0 of one final anisotropic electron population. For each event, this allows us to check the likelihood of a formation of the observed plateau by the observed whistler mode wave generated by the initial temperature anisotropy alone. The modified components of the electron distribution (i.e., the beam and temperature anisotropy) are Maxwellian distributions, justifying to consider the classical entropy S given in equation (4).

As the above procedure still leaves some range of uncertainty for the inferred parameters (corresponding to the unknown magnitude of entropy variation), we can use additional considerations on the efficiency of energy transfer (from the initial electron distribution to the wave) as a function of energy, to further limit the parameter domain. Based on a comparison between cyclotron resonance diffusion surfaces and constant energy surfaces, the strongest energy transfer between transverse electron energy and whistler mode chorus waves mainly takes place when $v_{\perp} \geq v_{\parallel}$ for a realistic, smooth latitudinal distribution of chorus waves obtained from combined Van Allen Probes and Cluster satellites statistics (Agapitov et al., 2018; Horne & Thorne, 2003; Summers et al., 1998)—that is, when the wave amplitude does not increase too strongly with latitude. Therefore, the increase of the transverse PSD in the reconstructed initial distribution (as compared with the measured final PSD) should be mostly confined to $E_{\perp} \geq E_{\parallel,\text{Cyclotron}}$, with

$$E_{\parallel,\text{Cyclotron}} = 250 \text{ keV} \cdot \left(\frac{\Omega_{ce} - \omega}{\omega_{pe} \cos \theta} \right)^2 \left(\frac{\Omega_{ce}}{\omega} \cos \theta - 1 \right)$$

the minimum electron energy for cyclotron resonance with the considered wave having a wave normal angle θ (Mourenas et al., 2015). The transverse energy of electrons with smaller initial E_{\perp} should be much less quickly lost during wave generation (at least, well above a very narrow loss-cone for the considered events at McIlwain shells $L > 4$).

The first event has been described by Min et al. (2014) and the electron distributions during this event are shown in Figure 3a. There is a clear plateau of parallel electron phase space density at ~ 1 keV and a significant transverse temperature anisotropy over almost the entire observed energy range (we use measurements from the Electrostatic Analyzer McFadden et al., 2008 onboard THEMIS A spacecraft Angelopoulos, 2008). Min et al. (2014) have shown that this plateau is accompanied by quasi-parallel whistler mode waves and that the plateau energy is close to the electron energy for Landau resonance with these waves. We fit the transverse (see red curve) and parallel (see black curve) electron PSD by combinations of Maxwellian and kappa distributions and calculate the total drift energy density of the electron beam corresponding to the observed plateau. Next, we transfer this whole final beam drift energy back to the initial energy of the anisotropy of the electron population that could have generated (via cyclotron resonance) the observed waves in Landau resonance with the beam (blue curve in Figure 3a). By simply increasing the transverse temperature of the corresponding Maxwellian, we increase the transverse initial PSD (as compared with its final level) mainly above 5 keV—that is, for E_{\perp} near or above $E_{\parallel,\text{Cyclotron}} \sim 10$ keV. The ratio of the observed (final) and estimated/reconstructed (initial) anisotropies of the electron population in the energy range of cyclotron resonance with the waves, and the normalized difference $S_{\text{final}} - S_{\text{init}}$ of observed (final) and estimated (initial)

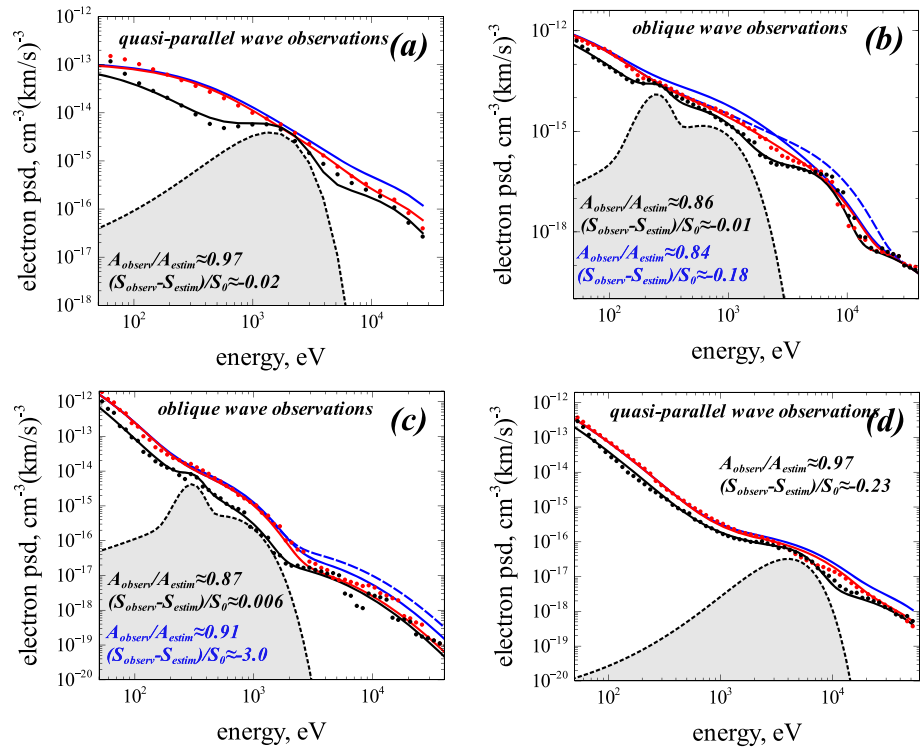


Figure 3. Four events of observations of electron plateau distributions and whistler mode waves: (a) Event with quasi-parallel whistler mode waves observed by THEMIS A on 10 March 2011 at 22:31:35–22:31:50 (Min et al., 2014); (b,c) events with very oblique whistler mode lower-band chorus waves observed by Van Allen Probe A on 3 December 2012 at 04:42:30–04:43:10, and on 12 May 2013 at 22:35:50–22:36:10 (Li, Mourenas, et al., 2016); (d) event with quasi-parallel whistler mode waves observed by Van Allen Probe A on 6 December 2015 at 07:15:00–07:30:00 (Li et al., 2019). Red and black circles show the measured transverse and parallel electron phase space densities, red and black curves show fits to these observations, gray curves shows the electron beam distribution allowing to fit the observed plateau, and blue curves show the transverse electron PSD with an increased anisotropy recalculated/reconstructed by including the energy of the (final) beam distribution. Solid and dashed blue curves show two different options of increased transverse PSD, mainly at low or high energy, respectively. The anisotropy ratio and normalized entropy difference of the observed (final) S_{observ} and reconstructed (initial) S_{estim} electron distributions are indicated in each panel (blue numbers corresponding to dashed blue curves).

classical entropies of the full electron distribution are indicated in Figure 3a. Our estimates suggest that this plateau distribution is unlikely to have been formed spontaneously by whistler mode waves generated by the initial anisotropic electron population, because such an energy transfer between cyclotron and Landau resonant electrons would correspond to a decrease of entropy.

Two other events of plateau observations accompanied by very oblique whistler mode lower-band chorus waves (taken from Li, Mourenas, et al., 2016) are shown in Figures 3b and 3c. In both cases, the electron distribution contains a very small and localized plateau near ~ 300 eV (we use measurements from the Helium, Oxygen, Proton, and Electron mass spectrometer Spence et al., 2013 onboard the Van Allen Probes Mauk et al., 2013). Note that Li, Mourenas, et al. (2016) have shown that the observed very oblique waves are in Landau resonance with the observed plateau. We fit the observed distributions and transfer the whole plateau/beam drift energy back to the (transverse) energy of the anisotropy of the electron population potentially interacting through cyclotron resonance with the observed waves, and which could have formed the plateau. For these two events, we test two different options for the reconstructed (initial) transverse PSD distributions, by increasing the perpendicular temperature mainly in the lower or higher energy range of the domain of cyclotron resonance with the waves. Increasing the transverse PSD mainly at low energy (at $E_{\perp} \geq 0.4$ keV, see solid blue curves in Figures 3b and 3c) corresponds for the event of Figure 3c to an increase of entropy from initial to final state, suggesting that the observed whistler mode waves could have formed the plateau through an energy transfer between the cyclotron and Landau resonant electron populations

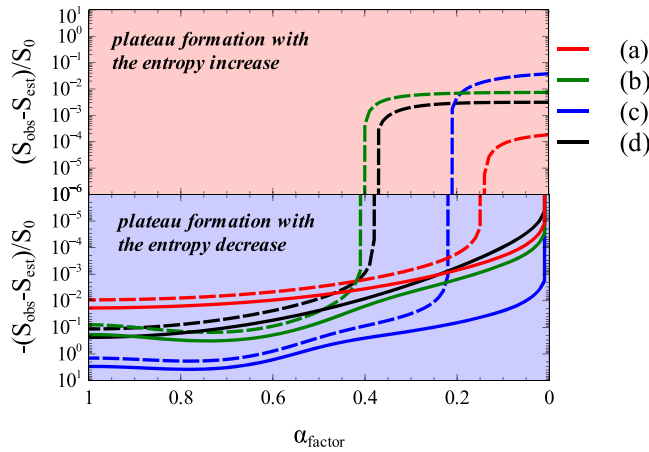


Figure 4. Difference between observed (final) and estimated (initial) entropies of the electron distribution for the four events in Figure 3, normalized to the entropy S_0 of one final anisotropic electron population, as a function of the fraction α_{factor} of the observed (final) beam drift energy assumed to have been transferred from the (initial) temperature anisotropy at higher energies. Solid lines show entropy evolution as a function of energy transfer fraction α_{factor} when all beam electrons have been accelerated by whistler mode chorus waves, and dashed lines show the same process but when only half of the beam electrons have been accelerated by these waves.

during this event. In contrast, the entropy decreases from initial to final state during the event of Figure 3b, indicating that this plateau/beam is unlikely to have been formed by the observed waves. Increasing the transverse PSD mainly at high energy (at $E_{\perp} > 0.7$ keV or at $E_{\perp} > 2$ keV, see dashed blue curves in Figures 3b and 3c) corresponds for both events to a decrease of entropy from initial to final states, suggesting that these plateau/beam distributions are unlikely to have been formed by whistler mode waves generated by the initial anisotropic electron population without beam. But which of these initial distributions is the most realistic?

As noted above, since the strongest energy transfer between transverse electron energy and chorus waves mostly occurs for $v_{\perp} \geq v_{\parallel}$ (Agapitov et al., 2018; Horne & Thorne, 2003; Summers et al., 1998), one expects the increase of the transverse PSD in the (reconstructed) initial distribution to be mostly limited to $E_{\perp} \geq E_{\parallel, \text{Cyclotron}}$, because lower E_{\perp} electrons will loose much less energy during wave generation. For the two events in Figures 3b and 3c, one finds $E_{\parallel, \text{Cyclotron}} \simeq 0.6$ keV and $\simeq 2.2$ keV, respectively (for $\omega/\Omega_{ce} \sim 0.32$ and 0.34 , $(\cos\theta - \omega/\Omega_{ce}) \sim 1/75$, and $\omega_{pe}/\Omega_{ce} \sim 8.5$ and ~ 4 , see Li, Mourenas, et al., 2016). On this basis, initial transverse electron distributions with PSD increases limited to the higher energy range (dashed blue curves) appear more realistic. This corresponds to a decrease of entropy from initial to final states in both events of Figures 3(b,c), suggesting that the very oblique chorus waves generated by the initial anisotropic electron population are unlikely to have formed these plateaus ab initio.

The last event of plateau distribution accompanied by quasi-parallel whistler mode chorus waves is shown in Figure 3d (this event has been previously described by Li et al., 2019). There is a clear plateau at ~ 4 keV. We fit the observed electron distribution (we use measurements from Helium, Oxygen, Proton, and Electron mass spectrometer, Spence et al., 2013 onboard the Van Allen Probes, Mauk et al., 2013) and transfer the whole plateau/beam drift energy back to the energy of the anisotropy of the electron population interacting through cyclotron resonance with the observed waves, which are also in Landau resonance with the plateau. Here, the transverse PSD is mainly increased for E_{\perp} near and above $E_{\parallel, \text{Cyclotron}} \simeq 15$ keV. Our estimates suggest that this plateau distribution is unlikely to have been formed by the whistler mode waves generated by the anisotropic electron population, because such an energy transfer between cyclotron and Landau resonant electrons would correspond to a decrease of entropy.

However, we have assumed in Figure 3 that the whole beam drift energy came from the anisotropy of the initial distribution. Actually, Landau resonant wave-driven electron acceleration produces a plateau distribution in parallel velocities by trapping electrons around Landau resonance (within the range of the trapping velocity proportional to the square root of the wave electric field) and by accelerating the initially more numerous electrons at parallel velocities smaller than the Landau resonant velocity up to higher parallel energies, where they increase the distribution, ultimately forming a plateau (e.g., Vedenov et al., 1962). Therefore, the (final) beam electrons are expected to have had a significant initial parallel velocity $v_{D, \text{init}}$, close to the minimum parallel velocity of the final plateau.

To take the finite initial parallel velocity $v_{D, \text{init}}$ of electrons into account, we hereafter assume that only a fraction $\alpha_{\text{factor}} < 1$ of the (final) beam drift energy has been transferred from the (initial) electron population. Conservation of total electron density requires to delete in the reconstructed (initial) distribution the final beam, and to add an *initial* beam population of the same density and similar temperature, but now with a *reduced* initial drift velocity $v_{D, \text{init}} = v_{D, \text{final}}(1 - \alpha_{\text{factor}})^{1/2}$.

Accordingly, we decrease in Figure 4 the fraction α_{factor} of final beam drift energy actually gained by electrons from Landau-resonant whistler mode waves, to check the consequences on the entropy variation in each of the four events of Figure 3 (considering only the more realistic higher-energy anisotropy increases in the two events with very oblique waves). Figure 4 (see solid curves) shows that for the four events, a production of the full beam by chorus wave-driven parallel acceleration would correspond to a decrease of the entropy,

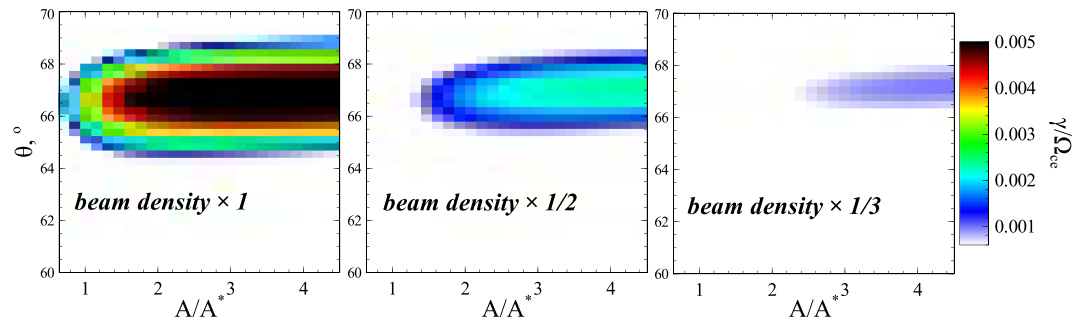


Figure 5. Linear growth rate of the observed very oblique whistler mode lower-band chorus waves in the event shown in Figure 3b for an electron distribution with reduced plateau/beam density (as compared with the beam shown by gray in Figure 3b): density reduction factor is 1, 1/2, and 1/3 for three panels from left to right. A/A^* is the ratio of electron anisotropy to marginal electron anisotropy for the measured background magnetic field and plasma parameters (see details in Li, Mourenas, et al., 2016). For this event, we have $\beta_{\parallel} = 4 \times 10^{-2}$ and $A^* \approx 2.36$.

even if only 10% of the final beam drift energy comes from the waves. Nevertheless, if only half of the beam electrons are accelerated by the same chorus waves, the entropy decreases only when $\alpha_{\text{factor}} > 0.2$ for events in Figures 3a and 3c and when $\alpha_{\text{factor}} > 0.4$ for events in Figures 3b and 3d. An inspection of plateaus in Figure 3 shows that they begin near $\sim 1/3$ of the beam drift energy for events in Figures 3(a,d), near $\sim 1/2$ of the beam drift energy for the event in Figure 3b, and near $\sim 1/1.5$ of the beam drift energy for the event in Figure 3c, leading to probable (realistic) α_{factor} values of 0.66, 0.5, and 0.3, respectively. All these values correspond to a decrease of entropy from initial to final states, even if only half of the beam electrons are accelerated by chorus waves. It confirms that the formation of the observed plateaus/beams in these four events is unlikely to have been caused by Landau resonance with the observed whistler mode waves.

The realistic α_{factor} values inferred from minimum plateau energies are closer to a domain of entropy increase for the two events with very oblique whistler mode waves in Figures 3b and 3c. But even if the observed plateau populations could potentially have been formed by the simultaneously observed very oblique waves, the generation of such waves would actually require a very strong initial anisotropy in the absence of a plateau. Indeed, to provide wave growth at high wave normal angles where Landau damping is strong without a plateau, cyclotron amplification needs to be stronger than Landau damping. However, Landau resonant electrons have generally much higher fluxes (at lower energy) than cyclotron resonant electrons, usually preventing oblique wave generation (Artemyev et al., 2016; Chen et al., 2013; Kennel et al., 1970).

To illustrate this point, Figures 5 show the growth rate of the observed very oblique waves (for the event in Figure 3b) for an initial electron distribution with a reduced plateau/beam density (as compared with its observed final density). We plot the growth rate as a function of electron anisotropy A normalized to the final, marginal anisotropy level $A^* = A_{\text{final}} = 2.36$. Considering a plateau/beam density merely reduced by factor $\sim 1/3$, we would need to start with an anisotropy exceeding the marginal stability level by more than a factor ≈ 3 –4 to overcome Landau damping and start the generation of very oblique waves with $\theta > 60^\circ$ as in observations (Li, Mourenas, et al., 2016). Moreover, the minimum energy $E_{\parallel, \text{Cyclotron}}$ of cyclotron resonance with parallel ($\theta = 0$) lower-band chorus waves is only ≈ 2 –4 times larger than for very oblique waves. Therefore, a strong increase of the anisotropy in the energy range favoring very oblique wave growth is also likely to favor parallel wave growth (initially prevented by a much weaker anisotropy and a strong Landau damping). Indeed, Figure 6 shows that for the huge initial anisotropy $A \approx 5A^*$ required for very oblique wave generation, the growth rate of parallel lower-band chorus waves would strongly exceed the growth rate of very oblique waves at similar frequencies. Such parallel waves would then largely dominate the energy transfer and much more quickly reduce the initial anisotropy than very oblique waves, likely hindering very oblique wave growth. Moreover, such parallel waves were not observed during this event. This suggests that a generation of the observed very oblique waves by the sole temperature anisotropy (without plateau/beam) is not realistic. It is much more probable that the plateau distribution was preexisting when the very oblique waves were generated.

Based on the above investigation, the observed plateau population is often likely to have been formed by some alternative mechanism—at least, not by the observed whistler mode waves alone. It is more probable that the observed whistler mode waves appear in Landau resonance with this plateau population mostly

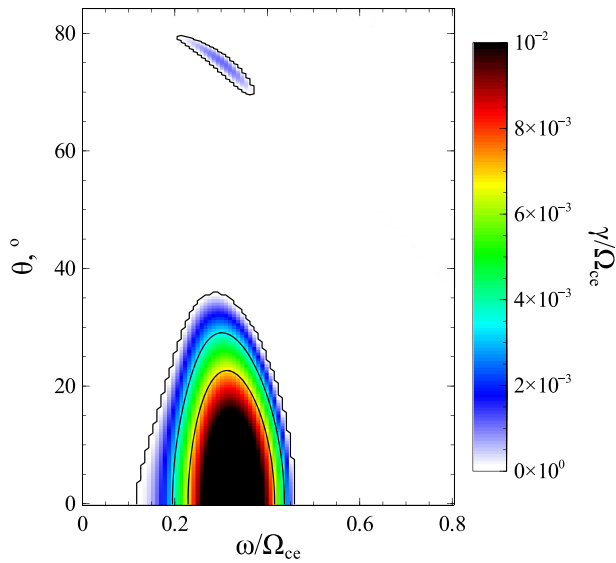


Figure 6. Growth rates of all whistler mode chorus waves in the presence of an electron distribution as the final distribution in Figure 3b but with a strongly increased anisotropy $A \approx 5A^*$ in the full energy range of cyclotron resonance with very oblique waves.

because such resonant waves are not damped (as suggested by Artemyev et al., 2016; Li, Mourenas, et al., 2016; Mourenas et al., 2015). Our estimates show that for quasi-parallel waves, the observed plateau distributions contain a too high energy to be generated by whistler mode waves alone (since such a generation would result in a decrease of entropy). During the events with very oblique lower-band chorus waves, some fraction (<50%) of the plateau distribution could be formed by the observed waves, but (i) this would require a very high (almost unrealistic) initial anisotropy to overcome the initially strong Landau damping and (ii) this would be inconsistent with the observed absence of additional, high amplitude parallel lower-band chorus waves that should be generated more efficiently by this same huge initial anisotropy (except in the case of a confinement of this huge anisotropy to a narrow low energy range, lower than the energy range for cyclotron resonance with parallel waves).

We caution that the above estimates do not pretend to provide a full description of the system—e.g., there could exist other initial distributions containing the energy of the observed plateaus but keeping a smaller entropy than the final distributions. Therefore, we leave a definitive answer to the question of the actual contribution of whistler mode waves to the formation of these observed plateaus for future self-consistent numerical simulations. Note, however, that such simulations should be performed in 2-D to describe the effect of wave propagation divergence,

and the use of such 2-D codes for self-consistent simulations of whistler mode wave growth and propagation has only recently started (Agapitov et al., 2018; Drake et al., 2015; Ke et al., 2017; Kuzichev et al., 2019; Lu et al., 2019; Ratcliffe & Watt, 2017).

4. Alternative Scenarios of Plateau Formation

Since the observed whistler mode waves are unlikely to form the observed plateaus in the electron velocity distribution, then some alternative mechanism(s) should exist. Such plateaus are seen principally for small pitch angle electrons and, thus, they could be formed by the relaxation of field-aligned electron beams. What could be the origin of such beams? The most widespread origin of electron beams observed in space plasma is a spatially localized field-aligned electric field, that is, a field-aligned potential drop generated either by DC electric fields (Lysak, 1990) or by low-frequency waves (Chaston et al., 2012; Lysak & Song, 2011) and nonlinear structures (Matsumoto et al., 1994). Let us consider below three possible origins of such electron beams with energies about the energy of Landau resonance with whistler mode waves.

4.1. Kinetic Alfvén Waves

Significant populations of intense whistler mode waves are observed around plasma injections into the inner magnetosphere (Khotyaintsev et al., 2011; Tao et al., 2011; Zhang et al., 2018), and the same injections are sources of ultralow frequency kinetic Alfvén waves (KAW) (Chaston et al., 2012; Ergun et al., 2015; Malaspina et al., 2015) that carry a significant field-aligned electric field (Lysak, 2008; Stasiewicz et al., 2000). This field-aligned electric field can effectively accelerate electrons along magnetic field lines (Damiano et al., 2015, 2016; Watt & Rankin, 2009, 2012) and form a field-aligned plateau in the electron distribution (Artemyev et al., 2015; Damiano et al., 2016). Electron acceleration by KAW can result in wave damping at high latitudes (Sharma Pyakurel et al., 2018), but around the equatorial plane KAWs are likely amplified by the unstable ion flow of the plasma injection. Such KAWs are widely observed and their energy is sufficiently important to heat ions (Chaston et al., 2014; Liang et al., 2016; Lin et al., 2017).

Figure 7 shows an example of plasma injection observed by THEMIS D (GSM coordinates are $x \sim -8R_E$, $y \sim 0.3R_E$). There is a strong KAW activity (broadband magnetic and electric fields around 03:42–03:44 UT) at the injection front seen as a jump of B_z field and electron spectra at $\sim 03:42:30$ UT (see also Malaspina et al., 2014, 2015). Electron distributions just behind the front show the formation of a plateau at energies ~ 100 – 300 eV at small pitch angles (compare panels (e) and (f)), and this plateau is continuously observed behind the front, where THEMIS also detected intense whistler mode emissions (see panels (c) and (d) with electric and magnetic spectra after 03:47 UT). For the observed whistler mode waves at a frequency $\omega \sim 0.15\Omega_{ce}$, the

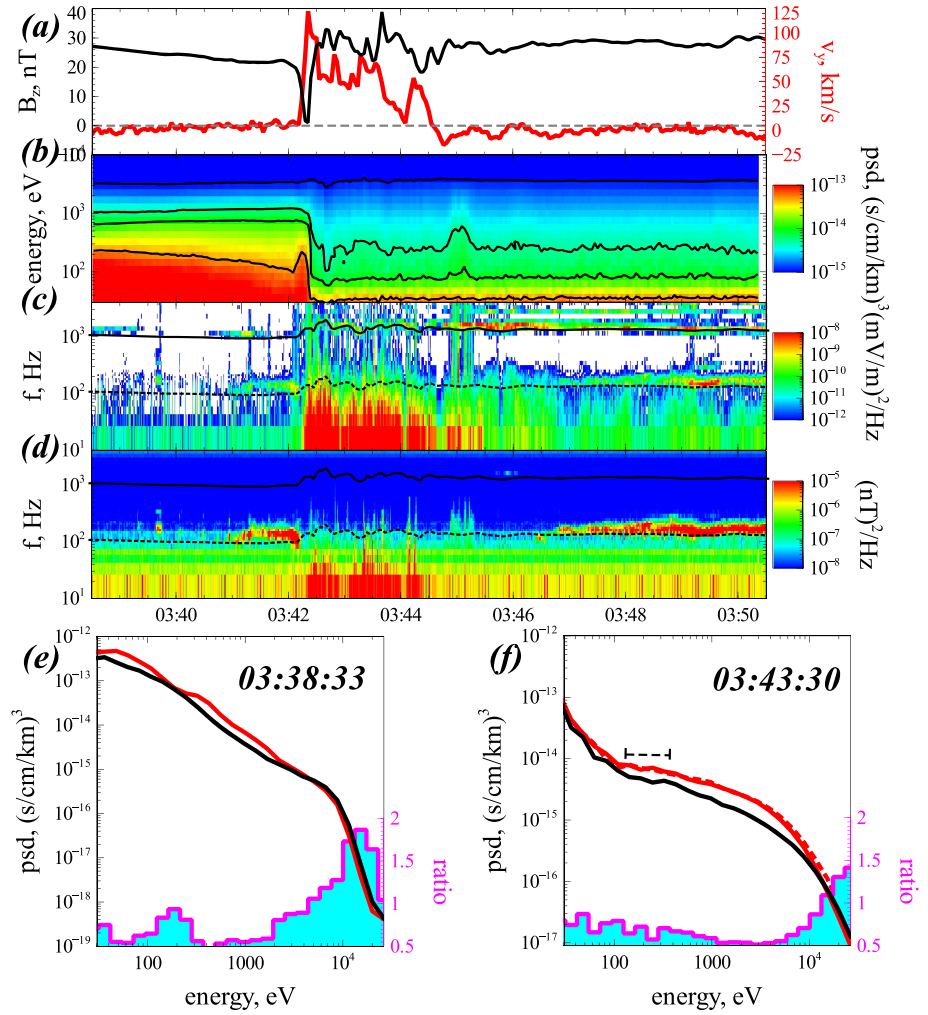


Figure 7. THEMIS D observations on 5 January 2017 (GSM coordinates $x \sim -8R_E$, $y \sim 0.3R_E$): (a) GSM B_z (black) and ion v_y (red) profiles (note that we use v_y as an indication of injection because at such a small radial distance ion duskward drift is stronger than earthward motion, (e.g., see Gabrielse et al., 2019); (b) electron phase space density measured by ESA (McFadden et al., 2008); (c, d) electric and magnetic spectra from the *fff* data set (Bonnell et al., 2008; Cully et al., 2008; Le Contel et al., 2008) with solid and dashed black lines showing f_{ce} and $0.1f_{ce}$; (e, f) electron spectra for transverse (black) and field-aligned (red) pitch angles. The dashed red curve in panel (f) shows the field-aligned PSD measured at 03:50 UT, when the most intense whistler mode waves are observed.

cold plasma dispersion gives a velocity for Landau resonance $v_{\parallel} = \omega/k \in [5, 10] \times 10^3$ km/s, corresponding to a parallel energy $(\omega/k)^2 m_e/2 \sim 150$ eV close to the plateau energy. Note that this plateau distribution has been formed well before the generation of whistler mode waves, but it is still observed during whistler mode emissions.

Let us compare the energy range $\sim E_{KAW}$ of electron acceleration by KAWs (i.e., the energies of plateau formation) and the energy of Landau resonance with whistler mode waves $E_{Landau} = v_{Landau}^2 m_e/2 \approx (\omega/k_{\parallel})^2 m_e/2$. The phase velocity of KAWs is quite small (about the Alfvén speed $\sim v_A$) in comparison with v_{Landau} , but the large electrostatic potential of KAWs significantly increases the resonance width (e.g., Damiano et al., 2016), leading to an energy range of electron acceleration $E_{KAW} \approx e\Phi$ and

$$E_{KAW} = e\Phi = \frac{eE_{\parallel,KAW}}{k_{\parallel,KAW}} \approx \frac{eE_{\perp,KAW}}{k_{\perp,KAW}} \frac{T_e}{T_i} \approx \frac{\Omega_{ce}}{\omega_{pe}} \sqrt{2T_i m_e c^2} \frac{T_e}{T_i} \frac{B_{\perp,KAW}}{B_0} \quad (5)$$

$$E_{Landau} = \frac{m_e}{2} \left(\frac{\Omega}{k_{\parallel}} \right)^2 = \frac{m_e c^2}{2} \frac{\Omega (\Omega_{ce} \cos \theta - \Omega)}{\omega_{pe}^2 \cos^2 \theta}$$

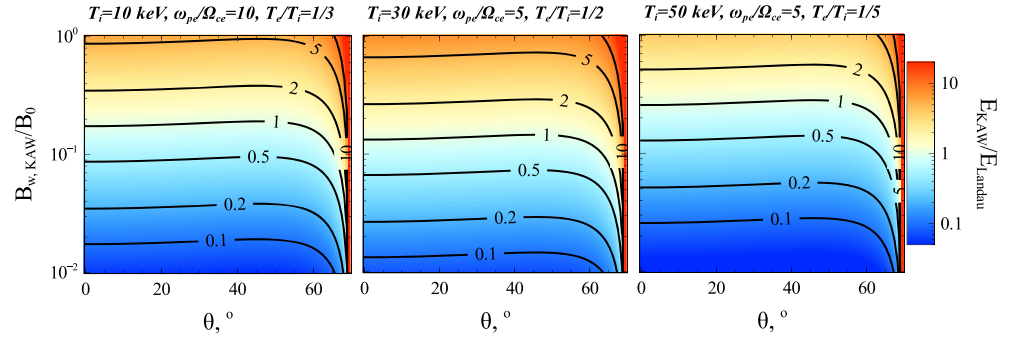


Figure 8. Energy ratio (6) for three sets of system parameters corresponding to plasma injections (low density): (left) near-Earth plasma sheet with $T_i \sim 10$ keV, $T_e \sim 3$ keV, $n_e \sim 1$ cm $^{-3}$, $B_0 \sim 30$ nT (see, e.g., Artemyev et al., 2016); (middle) the outer edge of the radiation belts $L \sim 7$ with $T_i \sim 30$ keV, $T_e \sim 15$ keV, $n_e \sim 1$ cm $^{-3}$, $B_0 \sim 60$ nT (see, e.g., Artemyev et al., 2018); (right) the ring current region with $T_i \sim 50$ keV, $T_e \sim 10$ keV, $n_e \sim 2.5$ cm $^{-3}$, $B_0 \sim 100$ nT (see, e.g., Yue et al., 2018). The whistler mode wave frequency is taken as $\omega = 0.35\Omega_{ce}$, corresponding to lower-band chorus waves.

where β_i is the ion beta (ratio of ion thermal pressure to magnetic field pressure) and we use $E_{\parallel,KAW}/E_{\perp,KAW} \approx (k_{\parallel,KAW}/k_{\perp,KAW})(T_e/T_i)$ and $cE_{\perp,KAW}/B_{\perp,KAW} \approx v_A k_{\perp,KAW} \rho_i$, where ρ_i is the ion gyroradius (see Chaston et al., 2003; Streltsov et al., 1998). The ratio E_{KAW}/E_{Landau} given by

$$\frac{E_{KAW}}{E_{Landau}} \approx \left(\frac{\omega}{\Omega_{ce}} \left(\cos \theta - \frac{\omega}{\Omega_{ce}} \right) \right)^{-1} \frac{\omega_{pe}}{\Omega_{ce}} \sqrt{\frac{8T_i}{m_e c^2} \frac{T_e}{T_i} \frac{B_{\perp,KAW}}{B_0} \cos^2 \theta} \quad (6)$$

is shown in Figure 8 as a function of $B_{\perp,KAW}/B_0$ and θ for different spatial domains (different β_i , T_e , Ω_{pe}/Ω_{ce} values). It turns out that sufficiently intense KAWs with $B_{\perp,KAW}/B_0 > 0.1$ – 0.2 can produce a plateau electron distribution allowing the generation of weakly oblique to very oblique whistler mode waves with negligible Landau damping within the injection regions, almost independently from the plasma conditions (within reasonable ranges of T_i , T_e , and ω_{pe}/Ω_{ce} parameters). Moreover, KAWs of lower amplitudes may still allow the generation of quasi-electrostatic very oblique whistler mode waves.

4.2. Time Domain Structures

Besides KAWs, strong field-aligned electric fields are associated with nonlinear electrostatic structures constituting the broadband electrostatic turbulence (Mozer et al., 2014, 2015). In the near-equatorial magnetosphere, such a turbulence mainly consists of electrostatic solitary waves (most likely electron acoustic solitons, see Agapitov et al., 2018; Vasko et al., 2017) and electron holes (Schamel, 1979; Vasko et al., 2017); a general name for these electrostatic fields is time domain structures (TDS) (Mozer et al., 2014, 2015). The typical velocity of these electrostatic structures is about the phase speed of electron acoustic waves $v_{EAW} \approx v_{e,hot}(n_{cold}/n_{hot})^{1/2}$ (see more accurate estimates in Vasko et al., 2017), that exist only in a two-temperature electron plasma with cold (density n_{cold} , temperature $T_{e,cold}$) and hot (density $n_{hot} > n_{cold}$, temperature $T_{e,hot}$) electron components (Gary & Tokar, 1985). TDS can effectively accelerate (Artemyev et al., 2014; Mozer et al., 2016; Vasko et al., 2016) and scatter (Vasko et al., 2018) electrons, forming a plateau population at energies $E_{TDS} \approx m_e v_{EAW}^2/2$ and even higher (if TDS accelerate electrons along an inhomogeneous background magnetic field, see Agapitov et al., 2018; Artemyev et al., 2017; Mozer et al., 2016).

Figure 9 shows one example of TDS and whistler mode wave observations around a plasma injection (a strong drop of low-energy electrons and a jump of B_z field; see similar observations in statistics of injections from Gabrielse et al., 2012; Malaspina et al., 2015). The electric field spectrum shows broadband electric field noise without a magnetic field counterpart (see panels (c) and (d)), that is, we indeed deal with an electrostatic turbulence. Within the region filled by this turbulence, the distribution of electrons is modified: there is a clear formation of a plateau population at ≈ 100 – 200 eV (compare panels (e) and (f)). Whistler mode waves, observed behind the injection front, propagate with a phase speed $\omega/k_{\parallel} \sim 7 \times 10^3$ km/s close to the speed of this plateau. As for the electron population observed around KAW emissions (see Figure 5), electrons interacting with TDS show an enhanced field-aligned phase space density over a wide energy range reaching up to ~ 1 keV. This may be the result of electron acceleration by TDS (or KAW) parallel electric

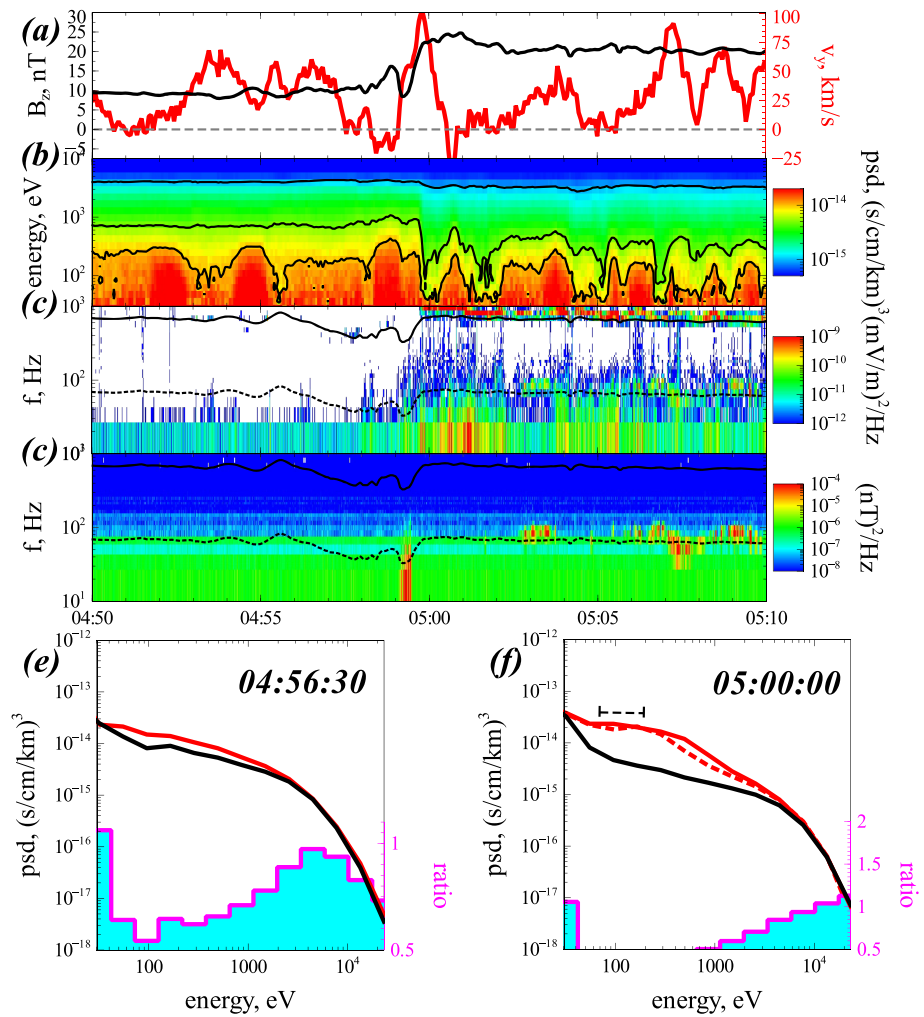


Figure 9. THEMIS E observations on 3 January 2017 (GSM coordinates are $x \sim -9R_E$, $y \sim -2R_E$): (a) GSM B_z (black) and ion v_y (red) profiles (note that we use v_y as an indication of injection because at such small radial distances the ion duskward drift is stronger than earthward motion, e.g., see Gabrielse et al., 2019); (b) electron PSD measured by ESA (McFadden et al., 2008); (c, d) electric and magnetic spectra from the *fff* data set (Bonnell et al., 2008; Cully et al., 2008; Le Contel et al., 2008) with solid and dashed black lines showing f_{ce} and $0.1f_{ce}$; (e, f) electron spectra for transverse (black) and field-aligned (red) pitch angles. The dashed red curve in panel (f) shows the field-aligned phase space density measured at the time 05:07:20 UT when the most intense whistler mode waves are observed.

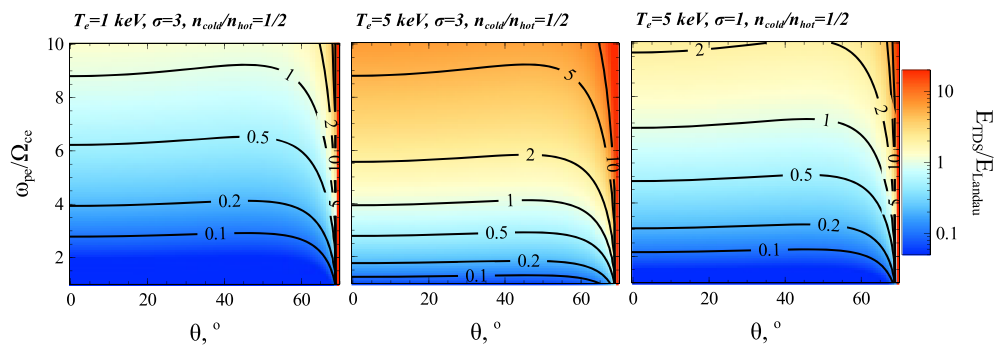


Figure 10. Energy ratio (7) for three sets of system parameters corresponding to plasma injections (low density; $n_{cold}/n_{hot} = 1/2$, see, e.g., Vasko et al., 2017): (left) cold plasma sheet with $T_e \sim 1$ keV and $\sigma = 3$; (middle) near-Earth hot plasma sheet $T_e \sim 5$ keV and $\sigma = 3$ (see, e.g., Artemyev et al., 2018); (right) same as in Figure 10 (middle), but with a very weak magnetic field gradient $\sigma = 1$ (the factor σ determines the increase of the background magnetic field magnitude within the latitude region where TDS propagate without significant damping, see discussions in Artemyev et al., 2014; Mozer et al., 2016; and Vasko et al., 2016). The whistler mode wave frequency is taken as $\omega/\Omega_{ce} = 0.35$.

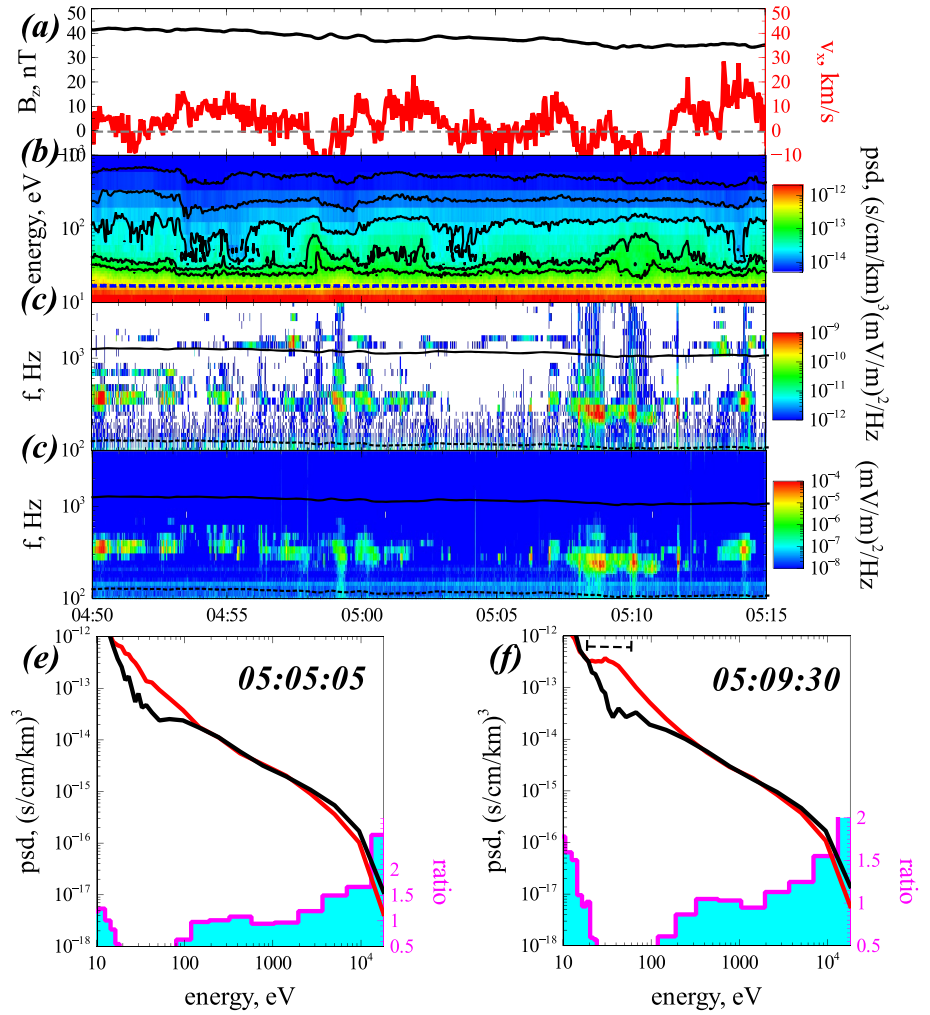


Figure 11. THEMIS A observations on 2 December 2016 (GSM coordinates are $x \sim -6.5R_E$, $y \sim -2.5R_E$): (a) GSM B_z (black) and ion v_z (red) profiles (note that due to the special mode of ESA operation with low energy resolution at >1 keV (Mozer et al., 2017), the plasma moments are quite noisy); (b) electron phase space density measured by ESA (McFadden et al., 2008); (c, d) electric and magnetic spectra from the *fff* data set (Bonnell et al., 2008; Cully et al., 2008; Le Contel et al., 2008); (e, f) electron spectra for transverse (black) and field-aligned (red) pitch angles.

fields in the inhomogeneous background magnetic field (see discussion in Artemyev et al., 2017 and results of Damiano et al., 2016; Mozer et al., 2016; Watt & Rankin, 2009).

Therefore, we consider $E_{\text{TDS}} = \sigma m_e v_{\text{EAW}}^2 / 2$ where the factor $\sigma \in [1, 5]$ is included to take into account an increased acceleration in the magnetic field gradient. Comparing this energy with the energy for Landau resonance gives:

$$\frac{E_{\text{TDS}}}{E_{\text{Landau}}} \approx \frac{\sigma T_{e,\text{hot}} n_{\text{cold}}}{m_e c^2 n_{\text{hot}}} \frac{\omega_{\text{pe}}^2 \cos^2 \theta}{\omega (\Omega_{\text{ce}} \cos \theta - \omega)} \quad (7)$$

Figure 10 shows that electron acceleration by TDS can form a plateau population in Landau resonance with very oblique whistler mode waves in the region of plasma injections, even for a very small magnetic field (very large $\omega_{\text{pe}}/\Omega_{\text{ce}} > 10$). For $\omega_{\text{pe}}/\Omega_{\text{ce}} \sim 5\text{--}10$ levels typical of near-Earth plasma injections (Zhang et al., 2018) TDSs can form a plateau that could be in Landau resonance with either parallel or oblique whistler mode waves.

4.3. Ionospheric Outflow

Whistler mode waves (and electron cyclotron harmonic waves often observed around plasma injections, see Zhang & Angelopoulos, 2014) scatter hot (>1 keV) electrons into the ionosphere, and this results in

a production of secondary electrons with energies below 500 eV (Khazanov et al., 2014, 2017). The propagation of these electrons back toward the equatorial plane forms the so-called ionospheric outflow, well modeled in kinetic simulations (Khazanov et al., 2015). This outflow is predominantly composed of field-aligned cold electron fluxes, with a pitch angle distribution that becomes narrower farther away from the ionosphere. Local beam instabilities driven by these cold field-aligned beams can scatter and thermalize electrons (André & Eliasson, 1995; Ergun et al., 1993; Temerin & Cravens, 1990), and finally result in the formation of a field-aligned plateau electron population near the equatorial plane. Therefore, electron scattering toward the loss cone by whistler mode waves can form cold electron field-aligned plateau distributions as a result of ionosphere-magnetosphere interaction (Nishimura et al., 2015). Figure 11 shows a good example of this kind of distribution. THEMIS A observes strong whistler mode waves in the inner magnetosphere without injection (quiet B_z) and without low-frequency electromagnetic field fluctuations (KAW or TDS). However, the recorded whistler mode wave emissions are accompanied by observations of an electron plateau population at energies 20–70 eV. Note that the spacecraft potential is ~ 18 eV and the observed electron population is shifted by +18 eV—i.e., the actual plateau energies are ≈ 2 –52 eV. The energies of this plateau population are quite close to the energies predicted for ionospheric outflow (Khazanov et al., 2014, 2017) and are also similar to the energies of Landau resonance with whistler mode waves. Accurate measurements of such a low-energy electron population were made possible by an especially designed regime of THEMIS A ESA (Mozer et al., 2017) that was operating from November 2016 to June 2017. These observations suggest that the ionospheric outflow induced by electron scattering by equatorial whistler mode waves can be responsible for the formation of a cold electron plateau population.

5. Discussion and Conclusions

A simplified theoretical analysis of whistler mode wave generation and resonant interaction with electrons, combined with various satellite observations in the inner magnetosphere, shows that whistler mode waves excited by transverse anisotropy alone are generally unlikely to have formed the observed plateau electron distributions—at least not from the start. An ab initio formation of this plateau population by the observed (Landau resonant) whistler mode waves alone would in general require a decrease of entropy, which is impossible for closed systems, or an unrealistically high initial anisotropy confined to a narrow low-energy range. However, significant energy transfers from cyclotron resonant energetic electrons (from plasma sheet injections) to Landau resonant colder electrons via the mediation of whistler mode waves are still fully possible and most likely do exist (Shklyar, 2011b, 2017). But such energy transfers are simply not sufficiently intense in general to form the plateau electron distribution that often accompanies whistler mode waves (Chen et al., 2019; Li, Mourenas, et al., 2016; Li et al., 2019; Min et al., 2014). The noted correlations between plateau and whistler mode wave observations do not necessarily imply a causal link between them, but can instead suggest that there is some other phenomenon causing both plateau formation and whistler mode wave generation.

Two examples of whistler mode wave observations within regions of injections from the plasma sheet show that strong low-frequency electric fields (carried by kinetic Alfvén waves Malaspina et al., 2015 or TDS Mozer et al., 2015) can lead to the formation of an electron plateau distribution. Among the initially broadband whistler mode waves generated within such injection regions, the particular waves in Landau resonance with such a plateau population will be much less damped and more efficiently amplified. This provides an alternative explanation for the fact that observed whistler mode waves are often found to be in Landau resonance with a plateau electron population (Li, Mourenas, et al., 2016; Li et al., 2019; Min et al., 2014). Moreover, the very strong field-aligned electric fields of kinetic Alfvén waves (driven by the hot ion population, much more energetic than the electron population) can produce electron beams (Watt & Rankin, 2009) that, in turn, can drive oblique whistler mode wave generation (Li, Mourenas, et al., 2016; Mourenas et al., 2015; Sauer & Sydora, 2010). Such a scenario of coupling between kinetic Alfvén waves/TDS and whistler mode waves through the electron population resembles the mechanism of induced scattering in an unstable plasma (Galeev & Sagdeev, 1979) (indeed, there are observations of TDS and whistler mode wave coupling in the inner magnetosphere, e.g., see Agapitov et al., 2015). Although the primary region for kinetic Alfvén waves and TDS formation is the plasma injection region (the flow breaking region in the nightside magnetosphere, see Chaston et al., 2015; Ergun et al., 2015; Mozer et al., 2017), kinetic Alfvén waves are also excited around plasma boundaries well within the outer radiation belt (Chu et al., 2019; Malaspina et al., 2015), and thus can form electron plateau populations even at small L shells.

A third example of electron plateau formation suggests a possible role of the ionosphere in reshaping the electron distribution. Indeed, whistler mode wave generation and electron scattering toward the loss cone should result in the formation of outflowing populations of secondary electrons (Khazanov et al., 2015). Such populations of ~ 100 eV field-aligned electrons are observed on DMSP (Wing et al., 2019) and can change the equatorial electron distribution (Nishimura et al., 2015). The feedback of the ionosphere to electron precipitations by whistler mode waves is generally neglected in wave-particle interaction studies, but through this feedback, the ionosphere could change the electron population in the wave source region and, thus, control the characteristics of excited whistler mode waves. This question is particularly important for the investigation of whistler mode wave driven aurora (Kasahara et al., 2018; Liang et al., 2011; Nishimura et al., 2010, 2011) and for the general problem of magnetosphere-ionosphere coupling (Khazanov et al., 2019; Wendel et al., 2019).

To conclude, this study shows that the processes of whistler mode wave generation and interaction with suprathermal (~ 0.1 – 3 keV) electrons should not be considered in isolation from the other processes potentially influencing the electron distribution. This suprathermal electron population, principally important for whistler mode wave properties and interacting with these waves through Landau resonance, is generally unlikely to have been shaped in the form of the observed plateaus by the observed whistler mode waves alone. It is more likely that these plateaus are mainly formed by other types of waves, such as kinetic Alfvén waves or TDS. Therefore, new full 2-D simulations (with a realistically inhomogeneous magnetic field) and detailed investigations of the roles played by low-frequency waves and ionospheric feedback are required to address the question of whistler mode wave relation to electron plateau distributions.

Acknowledgments

A. V. A. acknowledges the support of NSF Grant 1914594, NASA Grant 80NSSC18K1112 and NASA Contract NAS5-02099 for the use of data from the THEMIS Mission, specifically J. W. Bonnell and F. S. Mozer for the use of EFI data, A. Roux and O. LeContel for use of SCM data, and K. H. Glassmeier, U. Auster, and W. Baumjohann for the use of FGM data (provided under the lead of the Technical University of Braunschweig and with financial support through the German Ministry for Economy and Technology and the German Center for Aviation and Space (DLR) under Contract 50 OC 0302). We gratefully acknowledge the use of THEMIS data (ESA, FGM, *fff* data set for EFI and SCM) obtained from <http://themis.ssl.berkeley.edu/>, and the Van Allen Probes HOPE data from http://www.rbsp-ect.lanl.gov/data_pub/. Data access and processing was done using SPEDAS V3.1, see Angelopoulos et al. (2019).

References

- Agapitov, O., Artemyev, A., Krasnoselskikh, V., Khotyaintsev, Y. V., Mourenas, D., Breuillard, H., & Rolland, G. (2013). Statistics of whistler mode waves in the outer radiation belt: Cluster STAFF-SA measurements. *Journal of Geophysical Research: Space Physics*, *118*, 3407–3420. <https://doi.org/10.1002/jgra.50312>
- Agapitov, O., Drake, J. F., Vasko, I., Mozer, F. S., Artemyev, A., Krasnoselskikh, V., & Reeves, G. D. (2018). Nonlinear electrostatic steepening of whistler waves: The guiding factors and dynamics in inhomogeneous systems. *Geophysical Research Letters*, *45*, 2168–2176. <https://doi.org/10.1002/2017GL076957>
- Agapitov, O. V., Krasnoselskikh, V., Mozer, F. S., Artemyev, A. V., & Volokitin, A. S. (2015). Generation of nonlinear electric field bursts in the outer radiation belt through the parametric decay of whistler waves. *Geophysical Research Letters*, *42*, 3715–3722. <https://doi.org/10.1002/2015GL064145>
- Agapitov, O. V., Mourenas, D., Artemyev, A. V., & Mozer, F. S. (2016). Exclusion principle for very oblique and parallel lower band chorus waves. *Geophysical Research Letters*, *43*, 11,112–11,120. <https://doi.org/10.1002/2016GL071250>
- Agapitov, O. V., Mourenas, D., Artemyev, A. V., Mozer, F. S., Hospodarsky, G., Bonnell, J., & Krasnoselskikh, V. (2018). Synthetic empirical chorus wave model from combined Van Allen Probes and Cluster statistics. *Journal of Geophysical Research: Space Physics*, *123*, 297–314. <https://doi.org/10.1002/2017JA024843>
- Albert, J. M., Tao, X., & Bortnik, J. (2013). Aspects of nonlinear wave-particle interactions. In *Dynamics of the Earth's radiation belts and inner magnetosphere* (pp. 255–264). Washington, DC: American Geophysical Union. <https://doi.org/10.1029/2012GM001324>
- An, X., Yue, C., Bortnik, J., Decyk, V., Li, W., & Thorne, R. M. (2017). On the parameter dependence of the whistler anisotropy instability. *Journal of Geophysical Research: Space Physics*, *122*, 2001–2009. <https://doi.org/10.1002/2017JA023895>
- André, M., & Eliasson, L. (1995). Some electron conic generation mechanisms. *Washington DC American Geophysical Union Geophysical Monograph Series*, *86*, 61. <https://doi.org/10.1029/GM086p0061>
- Angelopoulos, V. (2008). The THEMIS mission. *Space Science Reviews*, *141*, 5–34. <https://doi.org/10.1007/s11214-008-9336-1>
- Angelopoulos, V., Cruce, P., Drozdov, A., Grimes, E. W., Hatzigeorgiou, N., King, D. A., & Schroeder, P. (2019). The Space Physics Environment Data Analysis System (SPEDAS). *Space Science Reviews*, *215*, 9. <https://doi.org/10.1007/s11214-018-0576-4>
- Artemyev, A., Agapitov, O., Mourenas, D., Krasnoselskikh, V., Shastun, V., & Mozer, F. (2016). Oblique whistler-mode waves in the Earth's inner magnetosphere: Energy distribution, origins, and role in radiation belt dynamics. *Space Science Reviews*, *200*, 261–355. <https://doi.org/10.1007/s11214-016-0252-5>
- Artemyev, A. V., Agapitov, O., Mozer, F., & Krasnoselskikh, V. (2014). Thermal electron acceleration by localized bursts of electric field in the radiation belts. *Geophysical Research Letters*, *41*, 5734–5739. <https://doi.org/10.1002/2014GL061248>
- Artemyev, A. V., Angelopoulos, V., & Runov, A. (2016). On the radial force balance in the quiet time magnetotail current sheet. *Journal of Geophysical Research: Space Physics*, *121*, 4017–4026. <https://doi.org/10.1002/2016JA022480>
- Artemyev, A. V., Rankin, R., & Blanco, M. (2015). Electron trapping and acceleration by kinetic Alfvén waves in the inner magnetosphere. *Journal of Geophysical Research: Space Physics*, *120*, 10–305. <https://doi.org/10.1002/2015JA021781>
- Artemyev, A. V., Rankin, R., & Vasko, I. Y. (2017). Nonlinear Landau resonance with localized wave pulses. *Journal of Geophysical Research: Space Physics*, *122*, 5519–5527. <https://doi.org/10.1002/2017JA024081>
- Artemyev, A. V., Zhang, X. J., Angelopoulos, V., Runov, A., Spence, H. E., & Larsen, B. A. (2018). Plasma anisotropies and currents in the near-Earth plasma sheet and inner magnetosphere. *Journal of Geophysical Research: Space Physics*, *123*, 5625–5639. <https://doi.org/10.1029/2018JA025232>
- Bonnell, J. W., Mozer, F. S., Delory, G. T., Hull, A. J., Ergun, R. E., Cully, C. M., & Harvey, P. R. (2008). The electric field instrument (EFI) for THEMIS. *Space Science Reviews*, *141*, 303–341. <https://doi.org/10.1007/s11214-008-9469-2>
- Bortnik, J., Inan, U. S., & Bell, T. F. (2006). Landau damping and resultant unidirectional propagation of chorus waves. *Geophysical Research Letters*, *33*, L03102. <https://doi.org/10.1029/2005GL024553>

- Breuillard, H., Zaliznyak, Y., Agapitov, O., Artemyev, A., Krasnoselskikh, V., & Rolland, G. (2013). Spatial spreading of magnetospherically reflected chorus elements in the inner magnetosphere. *Annales Geophysicae*, *31*, 1429–1435. <https://doi.org/10.5194/angeo-31-1429-2013>
- Chaston, C. C., Bonnell, J. W., Carlson, C. W., McFadden, J. P., Strangeway, R. J., & Ergun, R. E. (2003). Kinetic effects in the acceleration of auroral electrons in small scale Alfvén waves: A FAST case study. *Geophysical Research Letters*, *30*(6), 1289. <https://doi.org/10.1029/2002GL015777>
- Chaston, C. C., Bonnell, J. W., Clausen, L., & Angelopoulos, V. (2012). Energy transport by kinetic-scale electromagnetic waves in fast plasma sheet flows. *Journal of Geophysical Research*, *117*, A9202. <https://doi.org/10.1029/2012JA017863>
- Chaston, C. C., Bonnell, J. W., Kletzing, C. A., Hospodarsky, G. B., Wygant, J. R., & Smith, C. W. (2015). Broadband low-frequency electromagnetic waves in the inner magnetosphere. *Journal of Geophysical Research: Space Physics*, *120*, 8603–8615. <https://doi.org/10.1002/2015JA021690>
- Chaston, C. C., Bonnell, J. W., & Salem, C. (2014). Heating of the plasma sheet by broadband electromagnetic waves. *Geophysical Research Letters*, *41*, 8185–8192. <https://doi.org/10.1002/2014GL062116>
- Chen, R., Gao, X., Lu, Q., & Wang, S. (2019). Unraveling the correlation between chorus wave and electron beam-like distribution in the Earth's magnetosphere. *Geophysical Research Letters*, *46*, 11,671–11,678. <https://doi.org/10.1029/2019GL085108>
- Chen, L., Thorne, R. M., Li, W., & Bortnik, J. (2013). Modeling the wave normal distribution of chorus waves. *Journal of Geophysical Research: Space Physics*, *118*, 1074–1088. <https://doi.org/10.1029/2012JA018343>
- Chu, X., Malaspina, D., Gallardo-Lacourt, B., Liang, J., Andersson, L., Ma, Q., & MacDonald, E. A. (2019). Identifying STEVE's magnetospheric driver using conjugate observations in the magnetosphere and on the ground. *Geophysical Research Letters*, *46*, 12,665–12,674. <https://doi.org/10.1029/2019GL082789>
- Cully, C. M., Ergun, R. E., Stevens, K., Nammari, A., & Westfall, J. (2008). The THEMIS digital fields board. *Space Science Reviews*, *141*, 343–355. <https://doi.org/10.1007/s11214-008-9417-1>
- Damiano, P. A., Johnson, J. R., & Chaston, C. C. (2015). Ion temperature effects on magnetotail Alfvén wave propagation and electron energization. *Journal of Geophysical Research: Space Physics*, *120*, 5623–5632. <https://doi.org/10.1002/2015JA021074>
- Damiano, P. A., Johnson, J. R., & Chaston, C. C. (2016). Ion gyroradius effects on particle trapping in kinetic Alfvén waves along auroral field lines. *Journal of Geophysical Research: Space Physics*, *121*, 10,831–10,844. <https://doi.org/10.1002/2016JA022566>
- Demekhov, A. G., Taubenschuss, U., & Santolik, O. (2017). Simulation of VLF chorus emissions in the magnetosphere and comparison with THEMIS spacecraft data. *Journal of Geophysical Research: Space Physics*, *122*, 166–184. <https://doi.org/10.1002/2016JA023057>
- Drake, J. F., Agapitov, O. V., & Mozer, F. S. (2015). The development of a bursty precipitation front with intense localized parallel electric fields driven by whistler waves. *Geophysical Research Letters*, *42*, 2563–2570. <https://doi.org/10.1002/2015GL063528>
- Ergun, R. E., Delory, G. T., Klementis, E., Carlson, C. W., McFadden, J. P., Roth, I., & Temerin, M. (1993). VLF wave growth from dispersive bursts of field-aligned electron fluxes. *Journal of Geophysical Research*, *98*, 3777–3787. <https://doi.org/10.1029/92JA02193>
- Ergun, R. E., Goodrich, K. A., Stawarz, J. E., Andersson, L., & Angelopoulos, V. (2015). Large-amplitude electric fields associated with bursty bulk flow braking in the Earth's plasma sheet. *Journal of Geophysical Research: Space Physics*, *120*, 1832–1844. <https://doi.org/10.1002/2014JA020165>
- Fu, X., Cowee, M. M., Friedel, R. H., Funsten, H. O., Gary, S. P., Hospodarsky, G. B., & Winske, D. (2014). Whistler anisotropy instabilities as the source of banded chorus: Van Allen Probes observations and particle-in-cell simulations. *Journal of Geophysical Research: Space Physics*, *119*, 8288–8298. <https://doi.org/10.1002/2014JA020364>
- Fu, X. R., Cowee, M. M., Liu, K., Peter Gary, S., & Winske, D. (2014). Particle-in-cell simulations of velocity scattering of an anisotropic electron beam by electrostatic and electromagnetic instabilities. *Physics of Plasmas*, *21*, 042,108. <https://doi.org/10.1063/1.4870632>
- Gabrielse, C., Angelopoulos, V., Runov, A., & Turner, D. L. (2012). The effects of transient, localized electric fields on equatorial electron acceleration and transport toward the inner magnetosphere. *Journal of Geophysical Research*, *117*, A10213. <https://doi.org/10.1029/2012JA017873>
- Gabrielse, C., Spanswick, E., Artemyev, A., Nishimura, Y., Runov, A., Lyons, L., & Donovan, E. (2019). Utilizing the Heliophysics/Geospace System Observatory to understand particle injections: Their scale sizes and propagation directions. *Journal of Geophysical Research: Space Physics*, *124*, 5584–5609. <https://doi.org/10.1029/2018JA025588>
- Galeev, A. A., & Sagdeev, R. Z. (1979). Nonlinear plasma theory. *Reviews of Plasma Physics* (Vol. 7). New York: Consultants Bureau.
- Gary, S. P. (2005). *The theory of plasma waves*. Cambridge atmospheric and space. Cambridge UK: Cambridge University Press.
- Gary, S. P., & Feldman, W. C. (1977). Solar wind heat flux regulation by the whistler instability. *Journal of Geophysical Research*, *82*(7), 1087. <https://doi.org/10.1029/JA082i007p01087>
- Gary, S. P., Kazimura, Y., Li, H., & Sakai, J. I. (2000). Simulations of electron/electron instabilities: Electromagnetic fluctuations. *Physics of Plasmas*, *7*(2), 448–456. <https://doi.org/10.1063/1.873829>
- Gary, S. P., & Li, H. (2000). Whistler heat flux instability at high beta. *The Astrophysical Journal*, *529*(2), 1131–1135. <https://doi.org/10.1086/308294>
- Gary, S. P., & Tokar, R. L. (1985). The electron-acoustic mode. *Physics of Fluids*, *28*, 2439–2441. <https://doi.org/10.1063/1.865250>
- Gary, S. P., & Wang, J. (1996). Whistler instability: Electron anisotropy upper bound. *Journal of Geophysical Research*, *101*, 10,749–10,754. <https://doi.org/10.1029/96JA00323>
- Horne, R. B., & Thorne, R. M. (2003). Relativistic electron acceleration and precipitation during resonant interactions with whistler-mode chorus. *Geophysical Research Letters*, *30*(10), 1527. <https://doi.org/10.1029/2003GL016973>
- Horne, R. B., Thorne, R. M., Shprits, Y. Y., Meredith, N. P., Glauert, S. A., Smith, A. J., & Decreau, P. M. E. (2005). Wave acceleration of electrons in the Van Allen radiation belts. *Nature*, *437*, 227–230. <https://doi.org/10.1038/nature03939>
- Kasahara, S., Miyoshi, Y., Yokota, S., Kasahara, Y., Matsuda, S., Kumamoto, A., & Shinohara, I. (2018). Pulsating aurora from electron scattering by chorus waves. *Nature*, *554*, 337–340. <https://doi.org/10.1038/nature25505>
- Katoh, Y. (2014). A simulation study of the propagation of whistler-mode chorus in the Earth's inner magnetosphere. *Earth, Planets, and Space*, *66*, 6. <https://doi.org/10.1186/1880-5981-66-6>
- Katoh, Y., & Omura, Y. (2007). Computer simulation of chorus wave generation in the Earth's inner magnetosphere. *Geophysical Research Letters*, *34*, L03102. <https://doi.org/10.1029/2006GL028594>
- Katoh, Y., & Omura, Y. (2013). Effect of the background magnetic field inhomogeneity on generation processes of whistler-mode chorus and broadband hiss-like emissions. *Journal of Geophysical Research: Space Physics*, *118*, 4189–4198. <https://doi.org/10.1002/jgra.50395>
- Katoh, Y., & Omura, Y. (2016). Electron hybrid code simulation of whistler-mode chorus generation with real parameters in the Earth's inner magnetosphere. *Earth, Planets, and Space*, *68*, 192. <https://doi.org/10.1186/s40623-016-0568-0>
- Ke, Y., Gao, X., Lu, Q., Wang, X., & Wang, S. (2017). Generation of rising-tone chorus in a two-dimensional mirror field by using the general curvilinear PIC code. *Journal of Geophysical Research: Space Physics*, *122*, 8154–8165. <https://doi.org/10.1002/2017JA024178>

- Kennel, C. F., Scarf, F. L., Fredricks, R. W., McGehee, J. H., & Coroniti, F. V. (1970). VLF electric field observations in the magnetosphere. *Journal of Geophysical Research*, *75*, 6136–6152. <https://doi.org/10.1029/JA075i031p06136>
- Khazanov, G. V., Chen, M. W., Lemon, C. L., & Sibeck, D. G. (2019). The magnetosphere-ionosphere electron precipitation dynamics and their geospace consequences during the 17 March 2013 storm. *Journal of Geophysical Research: Space Physics*, *124*, 6504–6523. <https://doi.org/10.1029/2019JA026589>
- Khazanov, G. V., Glocer, A., & Himwich, E. W. (2014). Magnetosphere-ionosphere energy interchange in the electron diffuse aurora. *Journal of Geophysical Research: Space Physics*, *119*, 171–184. <https://doi.org/10.1002/2013JA019325>
- Khazanov, G. V., Sibeck, D. G., & Zesta, E. (2017). Major pathways to electron distribution function formation in regions of diffuse aurora. *Journal of Geophysical Research: Space Physics*, *122*, 4251–4265. <https://doi.org/10.1002/2017JA023956>
- Khazanov, G. V., Tripathi, A. K., Sibeck, D., Himwich, E., Glocer, A., & Singhal, R. P. (2015). Electron distribution function formation in regions of diffuse aurora. *Journal of Geophysical Research: Space Physics*, *120*, 9891–9915. <https://doi.org/10.1002/2015JA021728>
- Khotyaintsev, Y. V., Cully, C. M., Vaivads, A., André, M., & Owen, C. J. (2011). Plasma jet braking: Energy dissipation and nonadiabatic electrons. *Physical Review Letters*, *106*, 165,001. <https://doi.org/10.1103/PhysRevLett.106.165001>
- Kimura, I. (1966). Effects of ions on whistler-mode ray tracing. *Radio Science*, *1*(3), 269–283.
- Kuzichev, I. V., Soto-Chavez, A. R., Park, J., Gerrard, A., & Spitkovsky, A. (2019). Magnetospheric chorus wave simulation with the TRISTAN-MP PIC code. *Physics of Plasmas*, *26*, 072,901. <https://doi.org/10.1063/1.5096537>
- Kuzichev, I. V., Vasko, I. Y., Soto-Chavez, A. R., Tong, Y., Artemyev, A. V., Bale, S. D., & Spitkovsky, A. (2019). Nonlinear evolution of the whistler heat flux instability. *The Astrophysical Journal*, *882*, 81. <https://doi.org/10.3847/1538-4357/ab3290>
- Le Contel, O., Retinò, A., Breuillard, H., Mirioni, L., Robert, P., Chasapis, A., & Saito, Y. (2016). Whistler mode waves and Hall fields detected by MMS during a dayside magnetopause crossing. *Geophysical Research Letters*, *43*, 5943–5952. <https://doi.org/10.1002/2016GL068968>
- Le Contel, O., Roux, A., Robert, P., Coillot, C., Bouabdellah, A., de La Porte, B., & Larson, D. (2008). First results of the THEMIS search coil magnetometers. *Space Science Reviews*, *141*, 509–534. <https://doi.org/10.1007/s11214-008-9371-y>
- Li, J., Bortnik, J., An, X., Li, W., Angelopoulos, V., Thorne, R. M., & Baker, D. N. (2019). Origin of two-band chorus in the radiation belt of Earth. *Nature Communications*, *10*, 4672. <https://doi.org/10.1038/s41467-019-12561-3>
- Li, W., Mourenas, D., Artemyev, A. V., Bortnik, J., Thorne, R. M., Kletzing, C. A., & Spence, H. E. (2016). Unraveling the excitation mechanisms of highly oblique lower band chorus waves. *Geophysical Research Letters*, *43*, 8867–8875. <https://doi.org/10.1002/2016GL070386>
- Li, W., Santolik, O., Bortnik, J., Thorne, R. M., Kletzing, C. A., Kurth, W. S., & Hospodarsky, G. B. (2016). New chorus wave properties near the equator from Van Allen Probes wave observations. *Geophysical Research Letters*, *43*, 4725–4735. <https://doi.org/10.1002/2016GL068780>
- Li, W., Thorne, R. M., Bortnik, J., Baker, D. N., Reeves, G. D., Kanekal, S. G., & Green, J. C. (2015). Solar wind conditions leading to efficient radiation belt electron acceleration: A superposed epoch analysis. *Geophysical Research Letters*, *42*, 6906–6915. <https://doi.org/10.1002/2015GL065342>
- Li, W., Thorne, R. M., Bortnik, J., Shprits, Y. Y., Nishimura, Y., Angelopoulos, V., & Bonnell, J. W. (2011). Typical properties of rising and falling tone chorus waves. *Geophysical Research Letters*, *38*, L14103. <https://doi.org/10.1029/2011GL047925>
- Liang, J., Lin, Y., Johnson, J. R., Wang, X., & Wang, Z. X. (2016). Kinetic Alfvén waves in three-dimensional magnetic reconnection. *Journal of Geophysical Research: Space Physics*, *121*, 6526–6548. <https://doi.org/10.1002/2016JA022505>
- Liang, J., Spanswick, E., Nicolls, M. J., Donovan, E. F., Lummerzheim, D., & Liu, W. W. (2011). Multi-instrument observations of soft electron precipitation and its association with magnetospheric flows. *Journal of Geophysical Research*, *116*, A06201. <https://doi.org/10.1029/2010JA015867>
- Lin, Y., Wing, S., Johnson, J. R., Wang, X. Y., Perez, J. D., & Cheng, L. (2017). Formation and transport of entropy structures in the magnetotail simulated with a 3-D global hybrid code. *Geophysical Research Letters*, *44*, 5892–5899. <https://doi.org/10.1002/2017GL073957>
- Lu, Q., Ke, Y., Wang, X., Liu, K., Gao, X., Chen, L., & Wang, S. (2019). Two-dimensional gcPIC simulation of rising-tone chorus waves in a dipole magnetic field. *Journal of Geophysical Research: Space Physics*, *124*, 4157–4167. <https://doi.org/10.1029/2019JA026586>
- Lu, Q., Zhou, L., & Wang, S. (2010). Particle-in-cell simulations of whistler waves excited by an electron κ distribution in space plasma. *Journal of Geophysical Research*, *115*, A02213. <https://doi.org/10.1029/2009JA014580>
- Lundin, B., & Krafft, C. (2001). On the similarity features of normalized frequency spectrograms of magnetospherically reflected whistlers. *Journal of Geophysical Research*, *106*(A11), 25,643–25,654. <https://doi.org/10.1029/2000JA000346>
- Lysak, R. L. (1990). Electrodynamic coupling of the magnetosphere and ionosphere. *Space Science Reviews*, *52*, 33–87. <https://doi.org/10.1007/BF00704239>
- Lysak, R. L. (2008). On the dispersion relation for the kinetic Alfvén wave in an inhomogeneous plasma. *Physics of Plasmas*, *15*(6), 062,901. <https://doi.org/10.1063/1.2918742>
- Lysak, R. L., & Song, Y. (2011). Development of parallel electric fields at the plasma sheet boundary layer. *Journal of Geophysical Research*, *116*, A00K14. <https://doi.org/10.1029/2010JA016424>
- Malaspina, D. M., Andersson, L., Ergun, R. E., Wygant, J. R., Bonnell, J. W., Kletzing, C., & Larsen, B. A. (2014). Nonlinear electric field structures in the inner magnetosphere. *Geophysical Research Letters*, *41*, 5693–5701. <https://doi.org/10.1002/2014GL061109>
- Malaspina, D. M., Claudepierre, S. G., Takahashi, K., Jaynes, A. N., Elkington, S. R., Ergun, R. E., & Kletzing, C. A. (2015). Kinetic Alfvén waves and particle response associated with a shock-induced, global ULF perturbation of the terrestrial magnetosphere. *Geophysical Research Letters*, *42*, 9203–9212. <https://doi.org/10.1002/2015GL065935>
- Malaspina, D. M., Wygant, J. R., Ergun, R. E., Reeves, G. D., Skoug, R. M., & Larsen, B. A. (2015). Electric field structures and waves at plasma boundaries in the inner magnetosphere. *Journal of Geophysical Research: Space Physics*, *120*, 4246–4263. <https://doi.org/10.1002/2015JA021137>
- Matsumoto, H., Kojima, H., Miyatake, T., Omura, Y., Okada, M., Nagano, I., & Tsutsui, M. (1994). Electrostatic solitary waves (ESW) in the magnetotail: BEN wave forms observed by GEOTAIL. *Geophysical Research Letters*, *21*, 2915–2918. <https://doi.org/10.1029/94GL01284>
- Mauk, B. H., Fox, N. J., Kanekal, S. G., Kessel, R. L., Sibeck, D. G., & Ukhorskiy, A. (2013). Science objectives and rationale for the radiation belt storm probes mission. *Space Science Reviews*, *179*, 3–27. <https://doi.org/10.1007/s11214-012-9908-y>
- Maxworth, A. S., & Golkowski, M. (2017). Magnetospheric whistler mode ray tracing in a warm background plasma with finite electron and ion temperature. *Journal of Geophysical Research: Space Physics*, *122*, 7323–7335. <https://doi.org/10.1002/2016JA023546>
- McFadden, J. P., Carlson, C. W., Larson, D., Ludlam, M., Abiad, R., Elliott, B., & Angelopoulos, V. (2008). The THEMIS ESA plasma instrument and in-flight calibration. *Space Science Reviews*, *141*, 277–302. <https://doi.org/10.1007/s11214-008-9440-2>
- Meredith, N. P., Horne, R. B., Sicard-Piet, A., Boscher, D., Yearby, K. H., Li, W., & Thorne, R. M. (2012). Global model of lower band and upper band chorus from multiple satellite observations. *Journal of Geophysical Research*, *117*, A10225. <https://doi.org/10.1029/2012JA017978>

- Millan, R. M., & Thorne, R. M. (2007). Review of radiation belt relativistic electron losses. *Journal of Atmospheric and Solar-Terrestrial Physics*, 69, 362–377. <https://doi.org/10.1016/j.jastp.2006.06.019>
- Min, K., Liu, K., & Li, W. (2014). Signatures of electron Landau resonant interactions with chorus waves from THEMIS observations. *Journal of Geophysical Research: Space Physics*, 119, 5551–5560. <https://doi.org/10.1002/2014JA019903>
- Mourenas, D., Artemyev, A. V., Agapitov, O. V., Krasnoselskikh, V., & Mozer, F. S. (2015). Very oblique whistler generation by low-energy electron streams. *Journal of Geophysical Research: Space Physics*, 120, 3665–3683. <https://doi.org/10.1002/2015JA021135>
- Mozer, F. S., Agapitov, O. A., Angelopoulos, V., Hull, A., Larson, D., Lejosne, S., & McFadden, J. P. (2017). Extremely field-aligned cool electrons in the dayside outer magnetosphere. *Geophysical Research Letters*, 44, 44–51. <https://doi.org/10.1002/2016GL072054>
- Mozer, F. S., Agapitov, O. A., Artemyev, A., Burch, J. L., Ergun, R. E., Giles, B. L., & Vasko, I. (2016). Magnetospheric multiscale satellite observations of parallel electron acceleration in magnetic field reconnection by fermi reflection from time domain structures. *Physical Review Letters*, 116, 145,101. <https://doi.org/10.1103/PhysRevLett.116.145101>
- Mozer, F. S., Agapitov, O., Artemyev, A., Drake, J. F., Krasnoselskikh, V., Lejosne, S., & Vasko, I. (2015). Time domain structures: What and where they are, what they do, and how they are made. *Geophysical Research Letters*, 42, 3627–3638. <https://doi.org/10.1002/2015GL063946>
- Mozer, F. S., Agapitov, O. V., Hull, A., Lejosne, S., & Vasko, I. Y. (2017). Pulsating auroras produced by interactions of electrons and time domain structures. *Journal of Geophysical Research: Space Physics*, 122, 8604–8616. <https://doi.org/10.1002/2017JA024223>
- Mozer, F. S., Agapitov, O., Krasnoselskikh, V., Lejosne, S., Reeves, G. D., & Roth, I. (2014). Direct observation of radiation-belt electron acceleration from electron-volt energies to megavolts by nonlinear whistlers. *Physical Review Letters*, 113, 035,001. <https://doi.org/10.1103/PhysRevLett.113.035001>
- Mozer, F. S., Artemyev, A., Agapitov, O. V., Mourenas, D., & Vasko, I. (2016). Near-relativistic electron acceleration by Landau trapping in time domain structures. *Geophysical Research Letters*, 43, 508–514. <https://doi.org/10.1002/2015GL067316>
- Ni, B., Thorne, R. M., Zhang, X., Bortnik, J., Pu, Z., Xie, L., & Gu, X. (2016). Origins of the Earth's diffuse auroral precipitation. *Space Science Reviews*, 200, 205–259. <https://doi.org/10.1007/s11214-016-0234-7>
- Nishimura, Y., Bortnik, J., Li, W., Liang, J., Thorne, R. M., Angelopoulos, V., & Bonnell, J. W. (2015). Chorus intensity modulation driven by time-varying field-aligned low-energy plasma. *Journal of Geophysical Research: Space Physics*, 120, 7433–7446. <https://doi.org/10.1002/2015JA021330>
- Nishimura, Y., Bortnik, J., Li, W., Thorne, R. M., Chen, L., Lyons, L. R., & Auster, U. (2011). Multievent study of the correlation between pulsating aurora and whistler mode chorus emissions. *Journal of Geophysical Research*, 116, A11221. <https://doi.org/10.1029/2011JA016876>
- Nishimura, Y., Bortnik, J., Li, W., Thorne, R. M., Lyons, L. R., Angelopoulos, V., & Auster, U. (2010). Identifying the driver of pulsating aurora. *Science*, 330, 81–84. <https://doi.org/10.1126/science.1193186>
- Omura, Y., Katoh, Y., & Summers, D. (2008). Theory and simulation of the generation of whistler-mode chorus. *Journal of Geophysical Research*, 113, 4223. <https://doi.org/10.1029/2007JA012622>
- Omura, Y., Nunn, D., & Summers, D. (2013). Generation processes of whistler mode chorus emissions: Current status of nonlinear wave growth theory. In *Dynamics of the Earth's radiation belts and inner magnetosphere*. Washington, DC: American Geophysical Union. <https://doi.org/10.1029/2012GM001347>
- Ratcliffe, H., & Watt, C. E. J. (2017). Self-consistent formation of a 0.5 cyclotron frequency gap in magnetospheric whistler mode waves. *Journal of Geophysical Research: Space Physics*, 122, 8166–8180. <https://doi.org/10.1002/2017JA024399>
- Sagdeev, R. Z., & Shafranov, V. D. (1961). On the instability of a plasma with an anisotropic distribution of velocities in a magnetic field. *Soviet Phys. JETP*, 12(1), 130–132. <https://doi.org/10.5194/angeo-26-3525-2008>
- Santolik, O., Gurnett, D. A., Pickett, J. S., Chum, J., & Cornilleau-Wehrin, N. (2009). Oblique propagation of whistler mode waves in the chorus source region. *Journal of Geophysical Research*, 114, A00F03. <https://doi.org/10.1029/2009JA014586>
- Sauer, K., & Sydora, R. D. (2010). Beam-excited whistler waves at oblique propagation with relation to STEREO radiation belt observations. *Annales Geophysicae*, 28, 1317–1325. <https://doi.org/10.5194/angeo-28-1317-2010>
- Schamel, H. (1979). Theory of electron holes. *Physica Scripta*, 20, 336–342. <https://doi.org/10.1088/0031-8949/20/3-4/006>
- Sharma Pyakurel, P., Shay, M. A., Haggerty, C. C., Parashar, T. N., Drake, J. F., Cassak, P. A., & Gary, S. P. (2018). Super-Alfvénic propagation and damping of reconnection onset signatures. *Journal of Geophysical Research: Space Physics*, 123, 341–349. <https://doi.org/10.1002/2017JA024606>
- Shklyar, D. R. (2011a). On the nature of particle energization via resonant wave-particle interaction in the inhomogeneous magnetospheric plasma. *Annales Geophysicae*, 29, 1179–1188. <https://doi.org/10.5194/angeo-29-1179-2011>
- Shklyar, D. R. (2011b). Wave-particle interactions in marginally unstable plasma as a means of energy transfer between energetic particle populations. *Physics Letters A*, 375, 1583–1587. <https://doi.org/10.1016/j.physleta.2011.02.067>
- Shklyar, D. R. (2017). Energy transfer from lower energy to higher-energy electrons mediated by whistler waves in the radiation belts. *Journal of Geophysical Research: Space Physics*, 122, 640–655. <https://doi.org/10.1002/2016JA023263>
- Shklyar, D. R., Chum, J., & Jiricek, F. (2004). Characteristic properties of Nu whistlers as inferred from observations and numerical modelling. *Annales Geophysicae*, 22, 3589–3606. <https://doi.org/10.5194/angeo-22-3589-2004>
- Shklyar, D. R., & Matsumoto, H. (2009). Oblique whistler-mode waves in the inhomogeneous magnetospheric plasma: Resonant interactions with energetic charged particles. *Surveys in Geophysics*, 30, 55–104. <https://doi.org/10.1007/s10712-009-9061-7>
- Spence, H. E., Reeves, G. D., Baker, D. N., Blake, J. B., Bolton, M., Bourdarie, S., & Thorne, R. M. (2013). Science goals and overview of the radiation belt storm probes (RBSP) energetic particle, composition, and thermal plasma (ECT) suite on NASA's Van Allen Probes mission. *Space Science Reviews*, 179, 311–336. <https://doi.org/10.1007/s11214-013-0007-5>
- Stasiewicz, K., Bellan, P., Chaston, C., Kletzing, C., Lysak, R., Maggs, J., & Wahlund, J. E. (2000). Small scale Alfvénic structure in the aurora. *Space Science Reviews*, 92, 423–533.
- Streltsov, A. V., Lotko, W., Johnson, J. R., & Cheng, C. Z. (1998). Small-scale, dispersive field line resonances in the hot magnetospheric plasma. *Journal of Geophysical Research*, 103(A11), 26,559–26,572. <https://doi.org/10.1029/98JA02679>
- Summers, D., Tang, R., Omura, Y., & Lee, D. H. (2013). Parameter spaces for linear and nonlinear whistler-mode waves. *Physics of Plasmas*, 20, 72,110. <https://doi.org/10.1063/1.4816022>
- Summers, D., Thorne, R. M., & Xiao, F. (1998). Relativistic theory of wave-particle resonant diffusion with application to electron acceleration in the magnetosphere. *Journal of Geophysical Research*, 103, 20,487–20,500. <https://doi.org/10.1029/98JA01740>
- Tao, X. (2014). A numerical study of chorus generation and the related variation of wave intensity using the DAWN code. *Journal of Geophysical Research: Space Physics*, 119, 3362–3372. <https://doi.org/10.1002/2014JA019820>
- Tao, X., Chen, L., Liu, X., Lu, Q., & Wang, S. (2017). Quasilinear analysis of saturation properties of broadband whistler mode waves. *Geophysical Research Letters*, 44, 8122–8129. <https://doi.org/10.1002/2017GL074881>

- Tao, X., Thorne, R. M., Li, W., Ni, B., Meredith, N. P., & Horne, R. B. (2011). Evolution of electron pitch angle distributions following injection from the plasma sheet. *Journal of Geophysical Research*, *116*, A04229. <https://doi.org/10.1029/2010JA016245>
- Temerin, M. A., & Cravens, D. (1990). Production of electron conics by stochastic acceleration parallel to the magnetic field. *Journal of Geophysical Research*, *95*(A4), 4285–4290. <https://doi.org/10.1029/JA095iA04p04285>
- Thorne, R. M. (2010). Radiation belt dynamics: The importance of wave-particle interactions. *Geophysical Research Letters*, *37*, L22107. <https://doi.org/10.1029/2010GL044990>
- Thorne, R. M., Li, W., Ni, B., Ma, Q., Bortnik, J., Chen, L., & Kanekal, S. G. (2013). Rapid local acceleration of relativistic radiation-belt electrons by magnetospheric chorus. *Nature*, *504*, 411–414. <https://doi.org/10.1038/nature12889>
- Tong, Y., Vasko, I. Y., Artemyev, A. V., Bale, S. D., & Mozer, F. S. (2019). Statistical study of whistler waves in the solar wind at 1 AU. *The Astrophysical Journal*, *878*, 41. <https://doi.org/10.3847/1538-4357/ab1ff05>
- Tsurutani, B. T., Lakhina, G. S., & Verkhoglyadova, O. P. (2013). Energetic electron (>10 keV) microburst precipitation, 5–15 s X-ray pulsations, chorus, and wave-particle interactions: A review. *Journal of Geophysical Research: Space Physics*, *118*, 2296–2312. <https://doi.org/10.1002/jgra.50264>
- Tsurutani, B. T., & Smith, E. J. (1979). Interplanetary discontinuities—Temporal variations and the radial gradient from 1 to 8.5 AU. *Journal of Geophysical Research*, *84*, 2773–2787. <https://doi.org/10.1029/JA084iA06p02773>
- Vasko, I. Y., Agapitov, O. V., Mozer, F. S., Artemyev, A. V., & Drake, J. F. (2016). Electron holes in inhomogeneous magnetic field: Electron heating and electron hole evolution. *Physics of Plasmas*, *23*, 052,306. <https://doi.org/10.1063/1.4950834>
- Vasko, I. Y., Agapitov, O. V., Mozer, F. S., Artemyev, A. V., Krasnoselskikh, V. V., & Bonnell, J. W. (2017). Diffusive scattering of electrons by electron holes around injection fronts. *Journal of Geophysical Research: Space Physics*, *122*, 3163–3182. <https://doi.org/10.1002/2016JA023337>
- Vasko, I. Y., Agapitov, O. V., Mozer, F. S., Bonnell, J. W., Artemyev, A. V., Krasnoselskikh, V. V., & Hospodarsky, G. (2017). Electron-acoustic solitons and double layers in the inner magnetosphere. *Geophysical Research Letters*, *44*, 4575–4583. <https://doi.org/10.1002/2017GL074026>
- Vasko, I. Y., Krasnoselskikh, V. V., Mozer, F. S., & Artemyev, A. V. (2018). Scattering by the broadband electrostatic turbulence in the space plasma. *Physics of Plasmas*, *25*, 72,903. <https://doi.org/10.1063/1.5039687>
- Vasko, I. Y., Krasnoselskikh, V., Tong, Y., Bale, S. D., Bonnell, J. W., & Mozer, F. S. (2019). Whistler fan instability driven by Strahl electrons in the solar wind. *The Astrophysical Journal Letters*, *871*, L29. <https://doi.org/10.3847/2041-8213/ab01bd>
- Vedenov, A. A. (1967). Theory of a weakly turbulent plasma. *Reviews of Plasma Physics*, *3*, 229.
- Vedenov, A. A., Velikhov, E., & Sagdeev, R. (1962). Quasilinear theory of plasma oscillations. *Nuclear Fusion Suppl*, *2*, 465–475.
- Watt, C. E. J., Degeling, A. W., & Rankin, R. (2013). Constructing the frequency and wave normal distribution of whistler-mode wave power. *Journal of Geophysical Research: Space Physics*, *118*, 1984–1991. <https://doi.org/10.1002/jgra.50231>
- Watt, C. E. J., & Rankin, R. (2009). Electron trapping in shear Alfvén waves that power the aurora. *Physical Review Letters*, *102*, 045,002. <https://doi.org/10.1103/PhysRevLett.102.045002>
- Watt, C. E. J., & Rankin, R. (2012). Alfvén wave acceleration of auroral electrons in warm magnetospheric plasma. *Washington DC American Geophysical Union Geophysical Monograph Series*, *197*, 251–260. <https://doi.org/10.1029/2011GM001171>
- Wendel, D. E., Khazanov, G. V., Tripathi, A. K., Singhal, R. P., & Zesta, E. (2019). Source of the bursty bulk flow diffuse aurora: Electrostatic cyclotron harmonic and whistler waves in the coupling of bursty bulk flows to auroral precipitation. *Journal of Geophysical Research: Space Physics*, *124*, 6669–6690. <https://doi.org/10.1029/2019JA026606>
- Wilder, F. D., Ergun, R. E., Goodrich, K. A., Goldman, M. V., Newman, D. L., Malaspina, D. M., & Holmes, J. C. (2016). Observations of whistler mode waves with nonlinear parallel electric fields near the dayside magnetic reconnection separatrix by the magnetospheric multiscale mission. *Geophysical Research Letters*, *43*, 5909–5917. <https://doi.org/10.1002/2016GL069473>
- Wilson, L. B., Sibeck, D. G., Breneman, A. W., Contel, O. L., Cully, C., Turner, D. L., & Malaspina, D. M. (2014). Quantified energy dissipation rates in the terrestrial bow shock: 2. Waves and dissipation. *Journal of Geophysical Research: Space Physics*, *119*, 6475–6495. <https://doi.org/10.1002/2014JA019930>
- Wing, S., Khazanov, G. V., Sibeck, D. G., & Zesta, E. (2019). Low energy precipitating electrons in the diffuse aurora. *Geophysical Research Letters*, *46*, 3582–3589. <https://doi.org/10.1029/2019GL082383>
- Yue, C., An, X., Bortnik, J., Ma, Q., Li, W., Thorne, R. M., & Kletzing, C. A. (2016). The relationship between the macroscopic state of electrons and the properties of chorus waves observed by the Van Allen Probes. *Geophysical Research Letters*, *43*, 7804–7812. <https://doi.org/10.1002/2016GL070084>
- Yue, C., Bortnik, J., Li, W., Ma, Q., Gkioulidou, M., Reeves, G. D., & Mitchell, D. G. (2018). The composition of plasma inside geostationary orbit based on Van Allen Probes observations. *Journal of Geophysical Research: Space Physics*, *123*, 6478–6493. <https://doi.org/10.1029/2018JA025344>
- Yue, C., Chen, L., Bortnik, J., Ma, Q., Thorne, R. M., Angelopoulos, V., & Spence, H. E. (2017). The characteristic response of whistler mode waves to interplanetary shocks. *Journal of Geophysical Research: Space Physics*, *122*, 10,047–10,057. <https://doi.org/10.1002/2017JA024574>
- Zhang, X., & Angelopoulos, V. (2014). On the relationship of electrostatic cyclotron harmonic emissions with electron injections and dipolarization fronts. *Journal of Geophysical Research: Space Physics*, *119*, 2536–2549. <https://doi.org/10.1002/2013JA019540>
- Zhang, X., Angelopoulos, V., Artemyev, A. V., & Liu, J. (2018). Whistler and electron firehose instability control of electron distributions in and around dipolarizing flux bundles. *Geophysical Research Letters*, *45*, 9380–9389. <https://doi.org/10.1029/2018GL079613>
- Zhang, Y. L., Matsumoto, H., & Omura, Y. (1993). Linear and nonlinear interactions of an electron beam with oblique whistler and electrostatic waves in the magnetosphere. *Journal of Geophysical Research*, *98*, 21,353–21,363. <https://doi.org/10.1029/93JA01937>
- Zhou, Q., Yang, C., He, Y., Liu, S., Gao, Z., & Xiao, F. (2019). Excitation of highly oblique lower band and upper band chorus by a loss cone feature and temperature anisotropy distribution. *Geophysical Research Letters*, *46*, 1929–1936. <https://doi.org/10.1029/2018GL081379>